9. NONLINEAR OPTICAL FREQUENCY CONVERSION TECHNIQUES

U. Simon and F. K. Tittel

Department of Electrical and Computer Engineering
Rice University
Houston, Texas

9.1 Introduction

Using classical light sources, transparent optical materials are essentially passive, unaffected by the light wave traveling through them. For very intense light fields such as laser light, however, the presence of light can indeed affect the properties of the medium. These changes can act back on the light itself in a nonlinear way. The nonlinear response of the medium can convert the laser light into new spectral components, for example, harmonics of the optical frequency and, when more than one frequency is present in the input wave, sum- and difference-frequencies.

The nonlinear response of transparent dielectric media can be described by expanding the dipole moment per unit volume P in a Taylor series in terms of the incident oscillating electrical field [1]:

$$P = \varepsilon_0(\chi_1 E + \chi_2 EE + \chi_3 EEE + \ldots), \tag{1}$$

where χ is the weakly dispersive dielectric susceptibility; ε_0 is the vacuum permeability; and E is the incident light field. Classically, the dielectric susceptibility can be viewed as the response of an electron driven by an electromagnetic field in an anharmonic potential well resulting from the interatomic electric field E_A in the solid. The interatomic field is on the order of 10^8 V/cm. For driving optical fields much weaker than E_A, the polarization response is essentially linear. This low-optical-intensity regime is covered by the χ_1 term, which is responsible for ordinary optical phenomena like reflection and absorption. For optical fields intense enough to drive the electron beyond the quadratic minimum of the interatomic potential, the response becomes increasingly nonlinear, as described by the higher-order susceptibility terms. The second-order susceptibility χ_2 is a third-rank tensor and must therefore vanish if the medium is symmetric under inversion through the center of symmetry. This term is responsible for second-harmonic sum- and difference-frequency generation. The χ_3 term is responsible, for example, for the

EXPERIMENTAL METHODS IN THE PHYSICAL SCIENCES
Vol. 29C

Raman effect, the Kerr effect, and third-harmonic generation. A comprehensive introduction to the basics of these phenomena can be found in references [1, 2].

The generation of new frequencies (via χ_2 and χ_3) is of extreme practical importance because, although there have been a large number of lasers demonstrated, each type of laser typically generates only one or a few optical frequencies, and only a few lasers have proved practical and commercially viable. The necessity of achieving new wavelengths and to develop practical tunable coherent light sources has led to the exploration of nonlinear optics. The essential goal of practical nonlinear frequency conversion is the efficient generation of new spectral components from the input frequencies. At microwave frequencies, the availability of diode rectifiers and other strongly nonlinear elements permit straightforward design of efficient "lumped" mixers, smaller than a wavelength in size. At optical frequencies, by contrast, nonlinear responses are quite weak, so that efficient mixing requires "distributed" devices many wavelengths long. Many of the practical problems associated with optical frequency mixing result from the distributed nature of the mixing process. In particular, the difference in phase velocities of the interacting waves of different frequencies in a nonlinear medium produces a phase difference that accumulates along the length of the device and can significantly limit the efficiency of the mixing process. Thus, special steps have to be taken in order to "phase-match" nonlinear processes (see Section 9.2.1).

Some 30 years after the first demonstration of frequency conversion from the red to the blue [3], nonlinear optical devices have widespread applications in fields as diverse as laser fusion, biomedical instrumentation, femtosecond spectroscopy, and precision metrology. Though nonlinear optical technology is now well into its fourth decade, a renaissance is under way, driven by improvements in solid-state laser and nonlinear optical material technology.

The availability of high-power semiconductor diode lasers [4] has opened the door to rapid advances in diode-pumped solid-state laser sources such as Nd:YAG, Nd:YLF, Er:YAG, Tm–Ho:YAG, and Yb:YAG. These lasers operate at various discrete near-infrared wavelengths between 946 and 2010 nm in CW, Q-switched, or modelocked operation. Highly stable single-frequency diode-pumped monolithic YAG lasers [5] provide the frequency and amplitude stability as well as the power level required for highly efficient nonlinear frequency conversion. Single-mode GaAlAs diode lasers followed by high-power broad-area or tapered semiconductor amplifiers [6, 7] also serve as intense pump laser sources for nonlinear frequency conversion in the visible and near-infrared wavelength range. The large gain bandwidth of Ti:Al_2O_3 lasers, whose output can be tuned from 0.7 to 1.06 μm, makes it possible to generate modelocked pulses as short as 10 femtoseconds [8] to pump nonlinear optical devices for applications in ultrafast time-resolved spectroscopy.

New and improved crystalline nonlinear optical materials, such as BBO, LBO, KTP, $KNbO_3$, MgO:$LiNbO_3$, $AgGaS_2$, and $AgGaSe_2$, which all meet the key

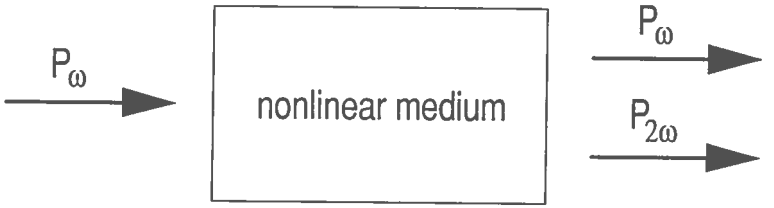

FIG. 1. Simple single-pass frequency doubling scheme. Part of the incident fundamental radiation P_ω is converted to the second harmonic $P_{2\omega}$.

requirements for efficient nonlinear optical frequency conversion, can be used to generate virtually any wavelength from the ultraviolet (UV) to the far-infrared (FIR). By using quasi-phase-matching (Section 9.2.5), virtually any nonlinear process can be phase-matched throughout the entire transparency range of the nonlinear optical crystal. The nonlinear frequency conversion efficiency can be significantly enhanced by introducing the nonlinear medium into the pump laser cavity (9.2.2) or a passive optical buildup cavity (9.2.3) that resonates the interacting light waves or by using guided-wave nonlinear optical devices (9.2.5).

A summary of progress in second-harmonic generation is given in Section 9.2. Section 9.3 describes sum- and difference-frequency mixing sources that can provide tunable radiation covering the entire wavelength region from the UV to the FIR. An overview of progress in third-harmonic generation is given in Section 9.4, followed by a description of optical parametric oscillators (OPOs) in Section 9.5. OPOs are unique in that they convert fixed-frequency lasers into coherent light sources tunable over extended wavelength regions. Stimulated Raman scattering (SRS) can be used to upshift and downshift the wavelength of tunable and fixed-frequency lasers (Section 9.6). Finally, up-conversion lasers (Section 9.7) pumped by near-infrared sources emit coherent radiation at shorter wavelengths (red to UV).

9.2 Second-Harmonic Generation

9.2.1 The Second-Harmonic Generation Process

In second-harmonic generation (SHG), the electric field of an incident light wave at frequency ω interacts with a nonlinear optical medium, giving rise to an output at twice the frequency of the incident radiation. Figure 1 illustrates the basic geometry of the SHG process. For plane waves and negligible pump power depletion, the generated harmonic intensity is given by [9]

$$P_{2\omega} = [KL^2P_\omega^2/A]\ \mathrm{sinc}^2(\Delta kL/2), \tag{2}$$

where $K = 2z^3\omega^2\varepsilon_0^2 d_{\text{eff}}^2$; $z = \sqrt{\mu_0/\varepsilon_0\varepsilon} = 377\Omega/n_0$ is the plane-wave impedance; n_0 is the refractive index of the nonlinear material; d_{eff} is the effective nonlinear coefficient; ε_0 is the vacuum permeability; P_ω is the incident fundamental power; A is the cross-section of the fundamental beam; L is the length of the nonlinear medium in the beam-propagation direction; and Δk is the wave–vector mismatch between the fundamental and harmonic wave.

The wave–vector mismatch Δk occurs because of the natural dispersion in the refractive index that is present in all materials. A plane wave at the fundamental frequency ω propagates with the phase velocity $c/n(\omega)$ through a nonlinear medium of length L, where $n(\omega)$ is the frequency-dependent refractive index. A polarization wave proportional to $\chi_2 E(\omega)E(\omega)$ is thus generated with twice the temporal and spatial frequency of the fundamental. This polarization wave serves as an oscillatory current density that generates the electromagnetic wave at frequency 2ω, propagating with phase velocity $c/n(2\omega)$. Quantum-mechanically, SHG involves the destruction of two photons at the fundamental frequency ω and generation of one photon at the second harmonic 2ω. The wave–vector mismatch Δk is thus given by:

$$\Delta k = k(2\omega) - 2k(\omega) = 4\pi(n_{2\omega} - n_\omega)/\lambda. \tag{3}$$

For the wave–vector mismatch $\Delta k \neq 0$, the generated harmonic wave gradually gets out of phase with the driving polarization as it propagates through the nonlinear medium (Fig. 2a). The relative phase of the interacting waves varies along the medium, and the direction of power flow oscillates, initially generating the second harmonic but then converting the second harmonic back into fundamental radiation after the relative phase reaches π. In this case, maximum conversion to the harmonic is obtained for a nonlinear medium whose length L is an odd multiple of the coherence length $L_c = \pi/\Delta k$. If $\Delta k = 0$, for example, $n_\omega = n_{2\omega}$, the phase velocities of the fundamental and second-harmonic waves are equal and the relative phase of the driving polarization and generated field remains constant throughout the nonlinear medium. The interaction is then said to be phase-matched and the harmonic power grows as the square of the length L (Fig. 2b).

Equation (2) indicates that in an interaction that is not phase-matched the efficiency is reduced by the factor $\text{sinc}^2(\Delta kL/2)$. For a typical coherence length of 5 μm, which corresponds to a reduction of $\sim 10^{-6}$ in a 1-cm nonlinear medium. For minimal reduction of the conversion efficiency, L_c must be larger than L. This requires matching the refractive indices to a part in 10^5 for L on the order of 1 cm. For typical media the indices differ by ~10% between the fundamental and the second harmonic. Thus, phase-matching does not occur without special steps.

A systematic approach to compensate for dispersion of the refractive index is quasi-phase-matching, which is discussed in Section 9.2.5. Most commonly, how-

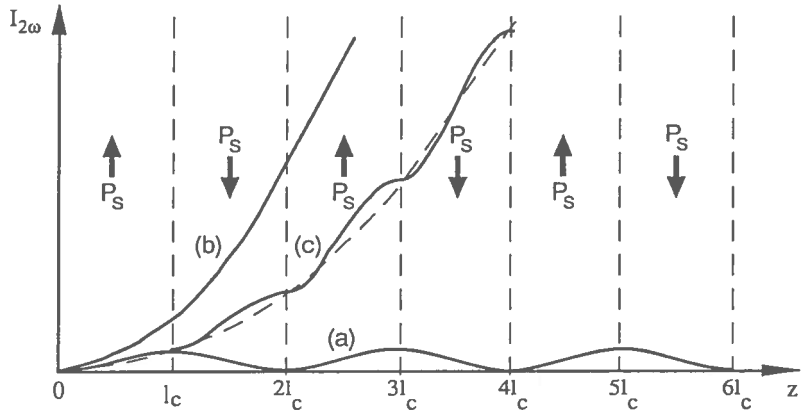

FIG. 2. The effect of phase-matching on the growth of second-harmonic intensity with distance in a nonlinear crystal; (a) nonphase-matched interaction; (b) perfect phase-matching in a uniformly poled crystal; (c) first-order QPM by flipping the orientation of the ferroelectric spontaneous polarization P_s (linked to the sign of the nonlinear coefficient) every coherence length for interaction curve (a) [37]. Reproduced with permission from the IEEE.

ever, SHG is phase-matched by exploiting the birefringence of nonlinear optical crystals. In uniaxial birefringent crystals, the two orthogonal polarization eigenmodes, known as ordinary and extraordinary waves, in general have different phase velocities: c/n_0 and c/n_e. Only the velocity of the extraordinary wave depends on the propagation direction in the crystal. In crystals with an appropriate balance of birefringence and dispersion, one can achieve phase-matching by choosing the propagation direction of the light such that the phase velocity of one polarization mode at the second-harmonic frequency is equal to that of the other polarization mode at the fundamental frequency (Fig. 3). This configuration is referred to as type I phase-matching. Thus, birefringent phase-matching makes use of those elements of the nonlinear susceptibility tensor χ_2 that couple orthogonally polarized waves. The value of Δk cannot only be adjusted by varying the angle Θ between the direction of propagation of the waves and the crystal optical axis but also by varying the temperature of the crystal for a fixed direction of propagation. The angle Θ at which $\Delta k = 0$ is called the phase-matching angle, and the temperature at which $\Delta k = 0$ and $\Theta = 90°$ is called the phase-matching temperature.

The usefulness of a particular nonlinear material for SHG is determined by the magnitude of its effective nonlinear coefficient and its ability to transmit and phase-match the harmonic and fundamental frequencies. The short wavelength limit of SHG (~205 nm by using BBO [10]) is currently set by an inability to phase-match the harmonic process at short wavelengths, while the infrared limit

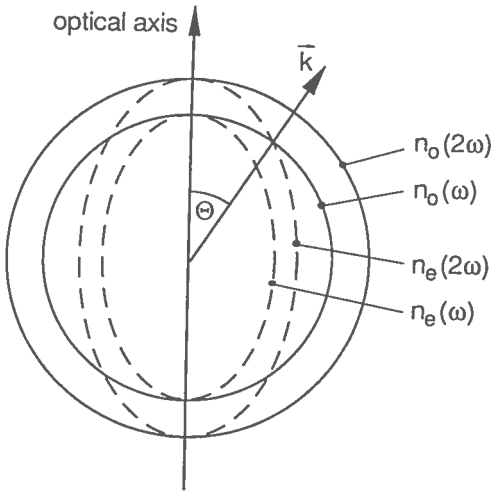

FIG. 3. Refractive index matching for SHG in a uniaxial positive birefringent crystal ($n_e < n_0$). At the phase-matching angle Θ between the beam propagation direction and the crystal optical axis the refractive indices of fundamental and harmonic match if they propagate as an *o*-ray and an *e*-ray, respectively.

is determined by increasing absorption at the fundamental. Some important properties of the most commonly used nonlinear optical crystals in SHG are summarized in Table I.

For phase-matched SHG with high fundamental intensities, the SHG intensity can grow so large that the depletion of the fundamental intensity must be accounted for. In this case, the SHG power is given by [9]

$$P_{2\omega} = P_{\omega} \tanh^2 [\sqrt{KL^2 P_{\omega}/A}\ \operatorname{sinc}(\Delta kL/2)] \,. \tag{4}$$

The inverse dependence of the conversion efficiency on the beam cross-section requires that the beam in practice be focused into the nonlinear crystal. A theoretical treatment of SHG for focused Gaussian beams was worked out by Boyd and Kleinman [11].

The SHG conversion efficiency is determined by parameters related to the pump source, such as power density, beam divergence, and spectral linewidth, and to the harmonic generator, such as nonlinear coefficient, crystal length, angular and thermal deviation from the optimum operating point, absorption, and inhomogeneities in the crystal. As indicated by Eq. (2), the conversion efficiency of the SHG process, $\eta = P_{2\omega}/P_{\omega}$, scales as the incident pump power if pump wave depletion is negligible. High-power continuous-wave (CW) or pulsed lasers are therefore easily converted with high efficiencies using a simple single-pass scheme

TABLE I. Properfies of Nonlinear Optical Materials

Material	Trans-parency [μm]	Effective nonlinear coefficient [pm/V]	Refrac-tive index @ 1064 nm	Pulsed damage threshold for 1-nsec pulses [GW/cm^2]	Absorp-tion [cm^{-1}] @ 1064 nm
KDP	0.18–1.8	0.44	1.49/1.46	5	0.07
$KTiOPO_4$ (KTP)	0.35–4.5	3.2	1.74/1.75/1.83	9–20	0.006
LiB_3O_5 (LBO)	0.16–2.3	0.85	1.56/1.59/1.61	20	0.005
β-BaB_2O_4 (BBO)	0.19–2.6	2	1.66/1.54	14	0.005
$KNbO_3$ (KN)	0.4–5.5	1.3	2.12/2.14/2.20	7	0.005
$LiNbO_3$	0.35–5	4.7	2.24/2.15	10	0.002
$LiNbO_3$	0.31–5	1.8	1.86/1.71	2	0.002
$AgGaS_2$	0.5–13	10.4	2.35/2.29	0.02 (10 ns)	0.09 @ 10.6 μm
$AgGaSe_2$	0.7–18	28	2.59/2.56	0.03 (50 nsec/2 μm)	0.05 @ 10.6 μm
$ZnGeP_2$	0.7–12	70	3.07/3.11	0.05 (25 nsec/2 μm)	0.9 @ 10.6 μm

[12], as shown in Fig. 1. However, in the case of low-power CW or diode-pumped CW modelocked lasers, the low single-pass doubling efficiency can be increased by two to three orders of magnitude either by resonantly enhancing the fundamental in the bulk nonlinear sample using a high-finesse resonator in either a passive or active configuration or by improving the optical confinement in the nonlinear medium with a single-pass waveguide structure.

9.2.2 Intracavity Frequency Doubling

For a laser resonator with an output coupler of transmission T, the intracavity circulating power is approximately a factor $1/T$ larger than the output power. Therefore, highly efficient harmonic conversion of low-power laser radiation can be achieved by placing the nonlinear crystal in an auxiliary beam waist of the laser cavity itself. In this case, the laser output coupler is replaced by a mirror that is highly reflective at the fundamental and highly transmissive at the harmonic. The doubler crystal inserted into the laser cavity acts as an output coupler of transmission T_{eff} in an analogous manner to the transmitting mirror of the normal laser, but couples out power at twice the laser frequency, $P_{2\omega} = T_{\text{eff}} P_\omega = \gamma P_\omega^2$, where $T_{\text{eff}} = \gamma P_\omega$. If the coupling parameter γ is chosen so that the conversion efficiency is equal to the optimum mirror transmission T of the fundamental laser, the available output at the fundamental will completely be converted to the harmonic [13]. For example, for a CW-pumped Nd:YAG laser with an optimum output coupling of $T = 0.1$,

an intracavity conversion efficiency of only 10% will produce an external conversion efficiency of 100%, so that the total 532-nm power generated in both directions by the doubler is equal to the maximum 1.064-μm power that can be extracted from the cavity without the nonlinear crystal.

In order to avoid degradation of the pump laser performance, high optical quality nonlinear crystals are required for intracavity frequency doubling. Moreover, spatial hole burning present in a standing-wave laser cavity allows the laser to operate in multiaxial mode. Since the losses of these axial modes are coupled through sum-frequency generation (Section 9.3) in the crystal, this gives rise to intrinsic large-amplitude fluctuations of the doubled output [14]. These instabilities can be eliminated by forcing the laser to oscillate in single-axial mode through the elimination of spatial hole burning or by using intracavity mode-selecting elements. The elimination of spatial hole burning can be accomplished by using either a unidirectional ring laser cavity [15, 16] or a twisted-mode linear resonator [17]. An example for stable intracavity frequency doubling of an Nd:YAG laser with an intracavity Brewster plate as a mode-selecting element [18] is shown in Fig. 4a. The fundamental is linearly *p*-polarized by the Brewster plate and is split by the KTP crystal into ordinary and extraordinary ray components, as shown in Fig. 4b. After traversing the KTP crystal, reflecting off the high reflector and passing through the crystal again, the wave returns to the Brewster plate with a phase difference $\delta = 4\pi\Delta n L_{KTP}/\lambda$ between the ordinary and extraordinary ray components, where L_{KTP} is the length of the KTP crystal, λ is the fundamental wavelength, and Δn is the birefringence of KTP at the fundamental. Only when δ is an integral multiple of π is the round-trip fundamental wave still *p*-polarized and transmitted by the Brewster plate without loss. With this setup, ~3 mW of stable green light at 532 nm was generated from 250 mW of incident diode laser pump power at 809 nm.

The number of intracavity components can be reduced by using a gain medium that also functions as the frequency-doubling nonlinear optical material (self-doubling NYAB; $Nd_xY_{1-x}Al_3(BO_3)_4$). In this case, the use of a monolithic laser cavity is particularly attractive for construction of a very compact diode laser-pumped CW laser source emitting at 531 nm [19]. However, since NYAB has an appreciable absorption at 531.5 nm that limits the useful crystal length, and since the thermally sensitive phase-matching process takes place in the presence of the pump-related thermal gradients, most reported NYAB laser outputs are low compared to the outputs of CW intracavity-doubled Nd:YAG lasers pumped at the same power level. Hemmati [20] reported 50 mW of CW 531-nm output power with an optical-to-optical conversion efficiency of 4% for a diode-pumped NYAB laser. Using the same pump laser, 140 mW of CW 532 nm was delivered from an Nd:YAG laser with an intracavity KTP doubler corresponding to 7% optical-to-optical conversion efficiency.

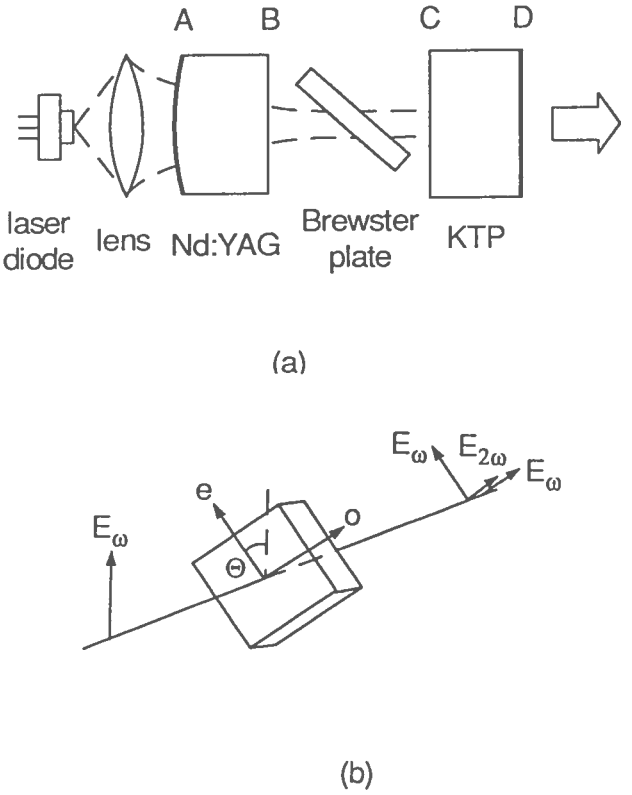

FIG. 4. (a) Design of an intracavity-doubled Nd:YAG laser with the Brewster plate and the KTP crystal serving as a frequency-selective birefringent filter [18]. Reproduced with permission from the IEEE. Facets A and D are HR-coated, and B and C are AR-coated for 1064 nm; A is AR-coated and B is HR-coated for the pump light at 809 nm; C is HR-coated and D is AR-coated for 532 nm. (b) Directions of the wave polarization and the birefringent crystal axes. The angle $\Theta = 45°$ is formed between the p-polarized light wave and the extraordinary ray in type II phase-matched KTP ($o \rightarrow e + o$).

9.2.3 External Enhancement Cavity

While intracavity frequency doubling has the advantage of being relatively easy to implement, it does not allow for independent optimization of the laser and doubling processes, a feature which is especially important in low-gain laser systems [21]. This degree of freedom is provided by the use of an external optical cavity to enhance the fundamental intensity inside the nonlinear crystal, a technique that was first demonstrated in 1966 by Ashkin *et al.* [22]. A well-designed cavity can increase the conversion efficiency by as much as three orders of

magnitude, making possible efficient devices with pump powers as small as 50 mW [23]. To couple the pump laser beam efficiently into the external resonator, the resonance of the enhancement cavity needs to be locked to the pump laser frequency [24, 25]. Thus, a frequency-stable single-axial-mode pump source and either an active servo cavity-length control scheme [26] or an optical feedback laser locking scheme [27] are required to maintain coincidence of the cavity resonance with the pump laser frequency. Moreover, only very low-loss doubling crystals and careful external cavity designs allow large fundamental enhancement factors to be achieved.

The theoretical treatment of external singly resonant SHG given in reference [22] was extended by Kozlovsky *et al.* [23] taking into account the effects of pump laser depletion. The harmonic power $P_{2\omega}$ generated by the circulating fundamental power P_c is given by

$$P_{2\omega} = \kappa \gamma_{2\omega} P_c^2, \tag{5}$$

where the parameter $\gamma_{2\omega}$ is the nonlinear conversion parameter, which can be derived using the formalism of Boyd and Kleinman [11] for focused Gaussian beams; κ is equal to 1 for a ring resonator and 2 for a standing-wave cavity. If r_m represents the fraction of resonated fundamental left after one round trip inside the cavity and $r_\omega = 1 - t_\omega$ is the fundamental input transmission of the cavity, the ratio of circulating power to input power is given by [23]

$$P_c/P_\omega = t_\omega / (1 - \sqrt{r_\omega r_m})^2 . \tag{6}$$

For a given geometry and input power, the amount of in-coupling t_ω must be chosen such that $r_m = r_\omega = 1 - t_\omega$, for example, the input transmission is equal to the total round-trip cavity loss including the depletion loss due to SHG [23]. This condition, for which the buildup factor is $P_c/P_\omega = 1/t_\omega$, corresponds to zero reflection for the fundamental and represents the optimum for second-harmonic conversion. The cavity is then said to be "impedance-matched", with all of the pump power driving the load and none being reflected. Proper impedance matching is critical for highly efficient SHG.

External Mirror Cavity Efficient resonant SHG requires that the total cavity round-trip loss of the resonated fundamental is dominated by harmonic conversion. It is the linear cavity losses (scatter and absorption) and not the magnitude of the nonlinear coupling constant that prevents achieving a conversion efficiency of 100%. A typical setup of an external cavity SHG experiment, using a bow-tie ring resonator [28], is shown in Fig. 5a. With a linear cavity round-trip loss of 1.7%, a fundamental power enhancement factor of 21 resulted in 36% SHG conversion efficiency at 18 W of CW 1.064-μm input pump power (Fig. 5b). A reduction in the linear cavity round-trip loss to 0.5% would increase the SHG

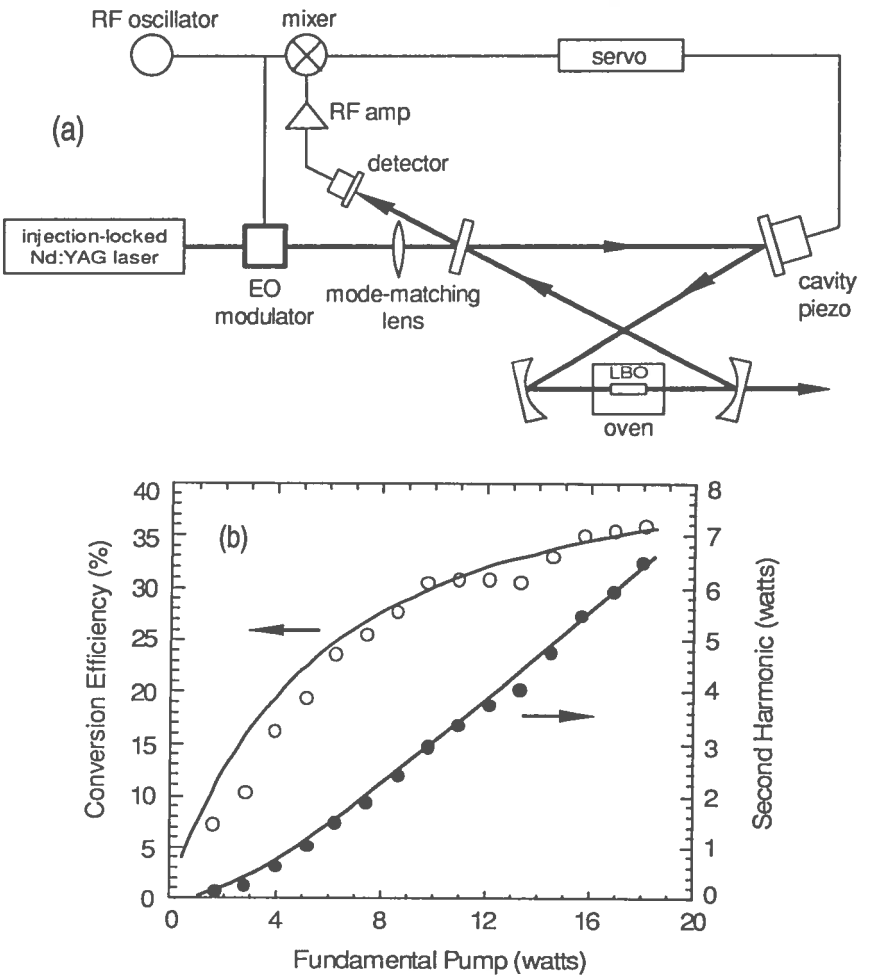

FIG. 5. (a) Experimental setup of a typical external SHG bow-tie cavity resonating an injection-locked Nd:YAG laser at 1.064 μm; (b) conversion efficiency and corresponding second-harmonic power as a function of the fundamental input power [28]. Reproduced with permission from the Optical Society of America.

conversion efficiency to 80% assuming perfect impedance and spatial mode matching into the external cavity. Using a very low-loss external ring cavity, SHG conversion efficiencies up to 85% have been achieved in 90° type II phase-matched KTP [29] for 700 mW of CW 1.08-μm input power [30]. The linear cavity losses of 0.32% were mainly due to the reflection losses at the surfaces of the crystal and resulted in a fundamental buildup factor of ~43.

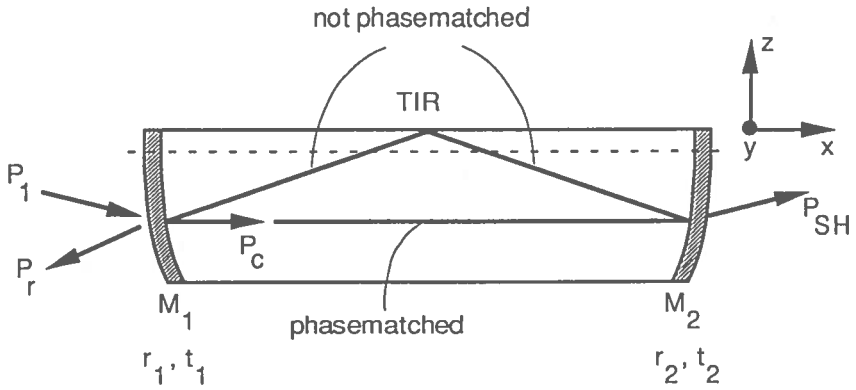

FIG. 6. Schematic diagram of a typical monolithic resonant frequency doubler. Mirrors are deposited directly onto the crystal, and a second harmonic is generated unidirectionally in the base leg of the regular beam path [31]. Reproduced with permission from the Society of Photo-Optical Instrumentation Engineers.

Monolithic Cavity In the case of a monolithic cavity design, the resonator is fabricated from a single piece of crystal with all radii, total internal reflection surfaces, and dielectric coatings directly formed on the crystal surfaces [31]. This technique minimizes losses and maximizes the rigidity of the resonator, yielding a highly stable and efficient narrow-linewidth device. The high passive frequency stability of these devices facilitates the locking of the laser frequency to the cavity. Either the pump laser frequency must be brought into coincidence with the cavity resonance or the intrinsic electrooptic and piezoelectric properties of the crystal, or a piezoelectric ceramic bonded to the monolithic resonator can be used to tune the cavity into resonance with the laser. Figure 6 shows a typical design of a monolithic ring resonator with spherical radii polished on each end of the crystal and a total internal reflection surface polished parallel to the mirror axis to define the ring resonator path. Only the base leg of the triangular beam path is phase-matched, and harmonic radiation is only generated in forward direction. The nonlinear crystal selected must be uniaxial with the resonated fundamental as the ordinary wave, or else the beam will bireflect at the mirrors whose reflection normals are not parallel or perpendicular to the *c*-axis of the nonlinear crystal. For the same reason, these resonators are not suitable for type II phase-matched SHG. A 12.5-nm MgO:$LiNbO_3$ monolithic ring cavity with a linear cavity round-trip loss of 0.42% and a fundamental power enhancement factor of 60 yielded 56% SHG conversion efficiency at 53 mW CW input power at 1.064 μm [23]. The same resonator device can be used as a standing-wave monolithic cavity by aligning the beam along the mirror axis. Both forward- and backward-propagating beams are then phase-matched, resulting in two harmonic outputs. An interesting variant of

this technique makes use of a monolithic ring Fabry–Perot resonator and total internal reflection to produce an extremely low-loss cavity that yields SHG of 1.064-μm beams with input power of less than 1 mW [32].

Devices are now commercially available that can generate more than 100 mW of 532-nm light by intra- or extracavity resonant SHG with diode-pumped Nd:YAG lasers as pump sources and either KTP or MgO:$LiNbO_3$ mixing crystals.

9.2.4 Synchronously Pumped Frequency Doubling

Resonant frequency-doubling schemes are also commonly used in the case of low-power CW modelocked lasers and have been theoretically described [33]. The picosecond-pulsed output of a modelocked laser described by Malcolm *et al.* [34] is impedance and spatially mode-matched into an external ring enhancement cavity that resonates the fundamental. The external ring cavity requires an active cavity-length stabilization scheme [26] with the round-trip time matched to the repetition rate of the modelocked laser so that adjacent pulses coincide in the external cavity and enhance the fundamental light. This is equivalent to matching the free spectral range (FSR) of the buildup cavity to the mode spacing of the modelocked laser. Two ring enhancement cavities in series using LBO and BBO as the doubling crystal, respectively, have been used to sequentially double (524 nm) and quadruple (262 nm) the frequency of a diode-pumped modelocked Nd:YLF laser [34]. With 1.4 W of CW modelocked Nd:YLF laser power (225-MHz repetition rate; 12-psec pulses) green output was generated with a 54% conversion efficiency, while the green-to-UV conversion efficiency was 11%.

9.2.5 Quasi-Phase-Matching

The essential difficulty in a nonphase-matched interaction is the difference in the phase velocities between the nonlinear polarization and the generated harmonic output, which produces a phase shift of π over every coherence length L_c, with a concomitant reversal of the energy flow between the waves (Fig. 2a). Birefringent phase-matching (Section 9.2.1) is the most commonly used technique to compensate for the phase velocity dispersion, but it limits the choice of useful SHG materials to those having an appropriate relationship between dispersion and birefringence and utilizes only those elements of the nonlinear susceptibility tensor that couple orthogonally polarized waves. Efficient birefringently phase-matched SHG has therefore been limited to a few nonlinear optical materials and a limited wavelength range. Phase-matching capabilities can be significantly extended by using quasi-phase-matching [35–37] (QPM). This technique involves repeated inversion of the relative phase between the driving polarization and the generated free harmonic by periodically resetting the phase of the polarization wave by π. This is accomplished by periodically varying the sign of the nonlinear coefficient

along the beam propagation direction and in synchronism with the generated harmonic. Figure 2c illustrates the effect of first-order QPM on the growth of harmonic intensity with distance in the nonlinear material. Using this technique, the interacting waves propagate at different phase velocities $v_{ph} = \omega/k$, but accumulated phase-mismatch is prevented. Therefore, power keeps flowing continuously from the fundamental to the harmonic output. The sign of the nonlinear coefficient is reversed spatially with a grating period $\Lambda = 2mL_c$, where $m = 1, 3, 5, \ldots$, is the QPM order; L_c is the coherence length, given by $L_c = \lambda/4(n_{2\omega} - n_\omega)$; λ is the wavelength of the fundamental; and the subscripts ω and 2ω refer to the fundamental and second-harmonic frequency, respectively. The QPM condition is $\mathbf{k}_{2\omega} - 2\mathbf{k}_\omega - \mathbf{K} = 0$, with $\mathbf{K}$ the wave vector of the nonlinear coefficient grating, having the magnitude $\mathbf{K} = 2m\pi/\Lambda$. The effective nonlinear coefficient for QPM is given by $d_{eff} = (2/m\pi)d_{ij}$, which indicates that the conversion efficiency for mth-order QPM is reduced by a factor of $(2/m\pi)^2$ as compared to perfect phase-matching. A more detailed theoretical treatment of QPM has been given by Fejer *et al.* [37]. The advantages of QPM result from the decoupling of phase-matching from the birefringence of the nonlinear material. QPM can phase-match virtually any nonlinear process at any temperature within the entire transparency range of a crystal, even if the crystal is isotropic. High conversion efficiencies can be achieved by taking advantage of any of the components of the nonlinear susceptibility tensor, including those coupling waves of the same polarization that allow the use of single-mode waveguide devices that support only one polarization. In the case of $LiNbO_3$, interactions involving wavelengths between 350 nm and 5 μm are possible utilizing a-axis grown $LiNbO_3$ and $d_{33} = 34$ μm/V, which is seven times larger than the birefringently phase-matchable d_{31}.

QPM in Bulk Devices The difficulty in implementing the QPM scheme lies in creating a medium with the requisite sign reversal every coherence length L_c, which, for visible interactions, is on the order of several microns. Early work for infrared interactions involved stacks of polished crystal plates, each being one coherence length thick with adjacent plates rotated by 180°. This technique has been demonstrated in such materials as CdTe [38], GaAs [39], $LiNbO_3$ [40], and later in LBO [41], but this proved to be difficult to handle and excessively lossy. A more practical approach is generation of a QPM grating of periodically inverted domains [42] in ferroelectric materials such as $LiNbO_3$ (periodically poled $LiNbO_3$, PPLN). This poling technique involves periodic perturbation of the growth conditions during crystal growth [43, 44], thereby patterning the nonlinear susceptibility. PPLN has been used for quasi-phase-matched SHG [45, 46]. An external SHG conversion efficiency of up to 42% was achieved for first-order QPM in a 1.24-nm a-axis-grown bulk sample of $LiNbO_3$ (domain length 3.47 μm) [46]. The PPLN crystal was placed inside an external bow-tie buildup cavity and

generated as much as 1.7 W of green, with 4.2 W of incident CW 1.064-μm Nd:YAG power. Up to an interaction length of 0.56 mm (160 domains), SHG conversion efficiency increased quadratically with crystal length, as expected for perfect domain periodicity.

QPM Using Surface Domain Gratings For a useful QPM device, the domain periodicity must be accurately controlled. If the spacing of the domains deviates from the ideal structure, a phase error accumulates between the interacting waves, resulting in a reduced nonlinear conversion efficiency [37]. Very precise lithographically controlled methods can be used to create QPM structures of alternating polarity at the surfaces of such ferroelectric substrates as $LiNbO_3$, $LiTaO_3$, or $KTiOPO_4$ (KTP). Using chemical gradients, periodic in-diffusion of dopants by means of a patterned mask induce domain reversals, thus achieving periodic poling on the wafer surface. Such surface domain gratings are used primarily in waveguide devices, which will be discussed in the next section. Moreover, the application of periodic fields with precise periodic electrodes is especially useful to pattern such centrosymmetric media as polymers [47] and liquids [48], in which second-order nonlinearity is induced by the applied electrical field.

QPM in Guided-Wave Devices The efficiency of single-pass bulk interactions is limited by the tradeoff between tight focusing for the sake of high intensities and loose focusing for the sake of large effective interaction lengths. Thus, for the frequency conversion of low-power lasers, often low-loss dielectric waveguides rather than bulk materials are used as the nonlinear media, as they allow strong modal confinement and thus high optical intensities over long interaction lengths. Compared to focused bulk interaction, the use of planar and channel waveguides improve the SHG conversion efficiency by factors of $(L/\lambda)^{1/2}$ and L/λ, respectively, where L is the length of the waveguide and λ the fundamental wavelength. This corresponds to improvement factors of 10^2 and 10^4, respectively, for SHG of 1-μm radiation in a 1-cm device. Thus, efficient nonresonant frequency conversion can be achieved with only milliwatts of pump power.

A channel waveguide nonlinear device is usually fabricated from a periodically poled planar nonlinear material wafer ($LiNbO_3$ [49, 50], $LiTaO_3$ [51–53], and KTP [54]). Waveguide fabrication requires creation of a core region of high refractive index surrounded by low-index cladding. In the oxide crystals widely used for frequency conversion, this as well can be accomplished by in-diffusing dopants into the wafer through a lithographic mask [49, 55]. Depending on the size and refractive index change of the core region, one or more modes are supported by the waveguide at a given wavelength [56]. Figure 7 depicts a typical channel waveguide device [52].

The advent of lithographic QPM techniques and compact diode laser pumps has stimulated much of the work on waveguide frequency conversion [37]. Con-

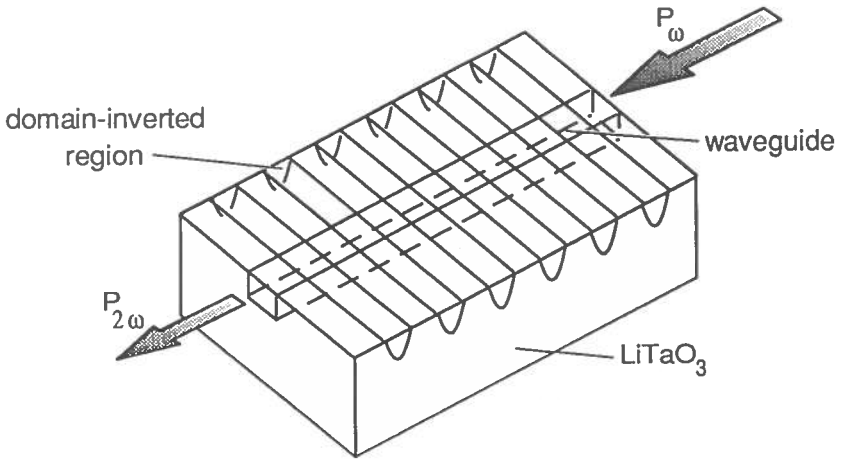

FIG. 7. Structure of a first-order quasi-phase-matched SHG $LiTaO_3$ waveguide [57]. Reproduced with permission from the Optical Society of America.

version efficiencies approaching 1% per mW have been demonstrated in 10-mm devices, and 10 to 20 mW of blue has been generated with pump powers below 100 mW by SHG in $LiNbO_3$, $LiTaO_3$, and KTP. Using a 10-nm first-order QPM $LiTaO_3$ SHG device, Yamamoto *et al.* [57] obtained 23 mW of blue light from 121 mW of Ti:Al_2O_3 laser input at 873 nm, corresponding to a normalized conversion efficiency ($\eta_{norm} = P_{2\omega}/(P_\omega L)^2$) of 157 %/W cm^2. Yamada *et al.* [58] reported the fabrication of a 3-mm periodic domain structure in a thin $LiNbO_3$ wafer by applying an external field at room temperature. After poling the substrate, a waveguide was fabricated in the first-order QPM SHG device using an annealed proton exchange process. As much as 20.7 mW of blue output was obtained for 196 mW of fundamental Ti:Al_2O_3 laser input power at 852 nm, corresponding to a normalized harmonic conversion efficiency of 600 %/W cm^2.

Waveguide QPM is not restricted to SHG. One can readily adapt this technology to a variety of interactions simply by changing the lithographic masks. It has already yielded SHG of wavelengths as short as 365 nm and difference-frequency generation (Section 9.3) of infrared wavelengths from 1.3 to 3 μm. Lim *et al.* [59] demonstrated quasi-phase-matched difference-frequency generation at 2 μm (1.8 μW) by mixing 1 mW from a 1.32-μm Nd:YAG laser with 160 mW from a tunable Ti:Al_2O_3 laser in a PPLN waveguide corresponding to a normalized conversion efficiency of 410 %/W cm^2. Laurell *et al.* [60] demonstrated efficient sum-frequency generation (Section 9.3) of two Ti:Al_2O_3 lasers in segmented KTP waveguides. For ~100 mW in each input beam, more than 2 mW of blue light was

generated between 390 and 480 nm with ~3-nm tunability and a maximum conversion efficiency of 84 %/W cm^2.

QPM opens the search for better nonlinear media to new classes of materials, such as poled-polymer and fused-silica films, diffusion-bonded stacks of plates, laterally patterned semiconductors, and asymmetric quantum wells. It is likely that these techniques will lead to significant progress in the performance of existing device types, as well as new devices that would not be possible with conventional media. For the near future, waveguide QPM holds out the promise of high-gain parametric amplification and CW parametric oscillation (Section 9.5).

9.3 Sum- and Difference-Frequency Generation

The general features and operating principles of sum- and difference-frequency generation are very similar to those discussed in detail in the previous section on SHG. As a matter of fact, SHG is a special case of sum-frequency generation (SFG), with the two incident photons having the same fundamental frequency ω.

9.3.1 Sum-Frequency Generation

SFG is used to up-convert two input pump sources with frequencies ω_1 and ω_2, generating a new frequency ω_3 according to the relation $\omega_3 = \omega_1 + \omega_2$. At low conversion efficiencies the generated intensity $I(\omega_3)$ grows as the product of the incident pump intensities $I(\omega_1)I(\omega_2)$. Complete conversion of the total radiation in both pump waves with perfect phase-matching is in principle possible if they start with an equal number of photons. Sum-frequency mixing is performed in the same types of nonlinear materials as used for SHG (Table I) and can generate tunable and fixed-frequency radiation from the near-vacuum ultraviolet (VUV) to the infrared region.

Generally, as two different wavelengths are combined in the SFG process, a wider frequency range can be covered by SFG than is accessible by SHG; especially the generation of short wavelengths below 200 nm becomes generally critical due to unattainable phase-matching for SHG (the SHG short-wavelength limit in BBO is 205 nm [61] and increasing absorption in all known nonlinear crystals. The first generation of CW coherent radiation below 200 nm was demonstrated by SFG in a KB_5 crystal [62]. With the invention of BBO as a new nonlinear material with excellent optical properties, this material became the most important optical crystal for the generation of short wavelengths down to 189 nm [61]. By mixing a tunable Ti:Al_2O_3 laser with a frequency-doubled Ar^+ laser (257 nm) in BBO, CW radiation tunable down to 191 nm was generated [63]. Output powers of more than 10 μW were obtained by resonating the Ti:Al_2O_3 laser in an external buildup cavity, and using a walkoff compensated crystal configuration

[64]. Using a doubly resonant cavity, coherent 194-nm radiation has been obtained with a CW output power of 31 μW [65].

Mückenheim *et al.* [66] demonstrated continuous coverage of the wavelength range from 189 to 197 nm by SFG in BBO using a tunable infrared dye laser (780 to 950 nm) and a frequency-doubled dye laser fixed to a wavelength of 245 nm. Peak energies of typically 10 to 100 μJ were obtained throughout this spectral range. More recently, by using a similar SFG-scheme Heitmann *et al.* [67] demonstrated generation of 100 μJ (20 kW) at 196 nm from 67-mJ Nd:YAG laser power used to pump two dye lasers. High output energies and conversion efficiencies could be achieved compared to competing methods for the generation of near-VUV radiation such as stimulated Raman scattering (~10 kW, $\eta \approx 10^{-2}\%$) [68] or four-wave difference-frequency generation and third-harmonic generation in rare gases (~20 to 60 W; $\eta \approx 10^{-4}\%$) [69].

The technique of SFG is also being used in the development of compact blue CW light sources based on near-infrared diode lasers. Resonantly enhanced SFG of several mW of blue light near 460 nm by mixing a single-mode diode laser with a diode-pumped 1064-nm Nd:YAG laser was demonstrated by using an intracavity SFG scheme [70] and by resonating both infrared pump lasers in an external monolithic KTP resonator [71].

Another application of SFG is the generation of the third and fourth harmonics of certain laser frequencies through two and three subsequent second-order parametric processes, respectively. Under certain conditions, these multistep processes are more efficient than direct third- or fourth-harmonic generation (Section 9.4). Nebel and Beigang [72] generated mW of VUV radiation tunable from 192 to 210 nm by SFG of the fundamental and third harmonic of a CW modelocked Ti:Al_2O_3 laser in BBO with a maximum conversion efficiency of $\eta_{4\omega} = P_{4\omega}/(P_{\omega}P_{3\omega})^{1/2}$ of ~4%.

9.3.2 Difference-Frequency Generation (DFG)

Difference-frequency mixing is used to down-convert radiation from two incident waves at frequencies ω_1 (pump) and ω_2 (signal) to a third wave at frequency ω_3 (idler) according to the relation $\omega_3 = \omega_1 - \omega_2$. In the low-conversion regime, as for SFG, the generated DFG intensity grows as the product of the pump intensities $I(\omega_1)I(\omega_2)$. Because mixing efficiency is proportional to the intensities of both the pump and the signal, the signal wave grows exponentially at the expense of the pump wave (until pump depletion sets in), a phenomenon known as parametric gain. DFG is an important technique for the generation of coherent tunable infrared radiation from CW and pulsed pump laser sources in the visible or near-infrared.

Early tunable CW DFG sources mixed a CW dye laser with its Ar^+ pump laser in temperature-tuned 90° type I phase-matched $LiNbO_3$ [73]. They proved very

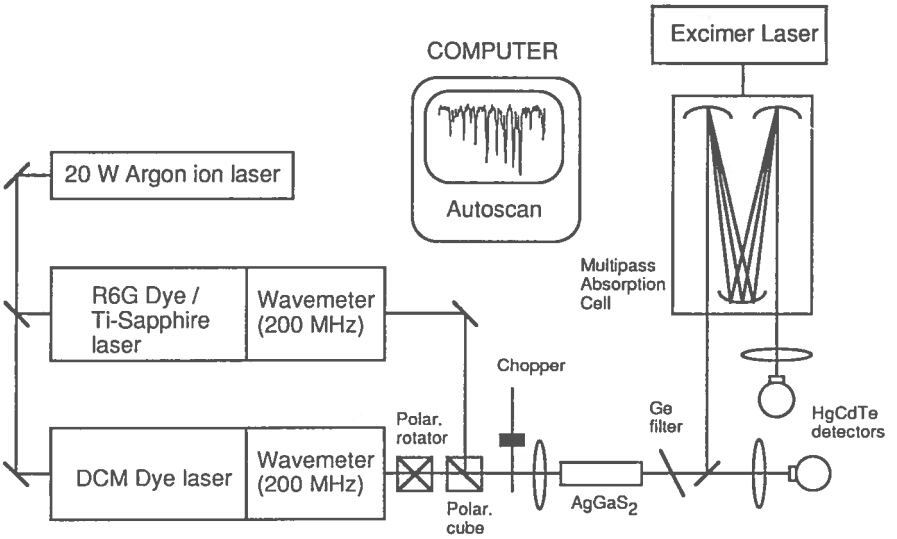

FIG. 8. Schematic of a DFG source used to generate continuously tunable narrow-band radiation from 3 to 9 μm utilizing type I noncritical phase-matching in $AgGaS_2$. The crystal is pumped by two dye and/or Ti:Al_2O_3 lasers [75]. Reproduced with permission from the Optical Society of America.

useful for high-resolution molecular spectroscopy but were limited to wavelengths shorter than 4 μm by the transmission characteristics of $LiNbO_3$. The use of $LiIO_3$ as the nonlinear medium extended the long-wavelength limit for CW DFG to ~5 μm [74]. Advances in nonlinear optical materials, such as $AgGaS_2$ and $AgGaSe_2$, now allow the generation of infrared radiation continuously tunable up to 18 μm by means of DFG, providing access to virtually all molecular fundamental vibrational modes. The narrow-band ($\delta\lambda \approx 1$ MHz) CW DFG source demonstrated by Canarelli *et al.* [75] was based on 90° type I phase-matching in $AgGaS_2$ and pumped by single-mode dye and/or Ti:Al_2O_3 lasers. It covered the infrared wavelengths from 4 to 9 μm with CW output powers of several 10 μW, exceeding the noise equivalent power (NEP) of liquid N_2-cooled infrared detectors by four to five orders of magnitude. The infrared source, shown schematically in Fig. 8, has been used to detect high-resolution kinetic spectra of such various free radical species as HOCO, DOCO, and HCCN [76].

Significant progress in the field of CW III–V semiconductor diode lasers [77] makes these sources attractive as pump lasers in compact and robust infrared CW DFG spectrometers for applications in chemical analysis, environmental sensing, industrial process monitoring, and medical technology. The nonlinear conversion efficiency of early all-diode laser CW DFG [78] has been limited by the low output

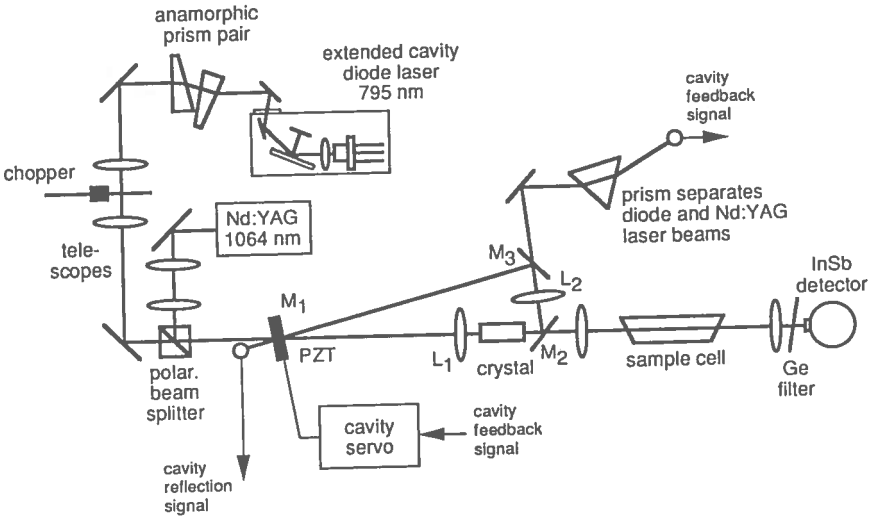

FIG. 9. Schematic of a DFG source used to generate infrared light near 3.2 μm by mixing an external-cavity diode laser (795 nm) with a compact diode-pumped Nd:YAG laser (1064 nm) in $AgGaS_2$. The 1064-nm radiation is enhanced by using a three-mirror buildup cavity. As much as 2 μW of IR has been generated and has been used to detect methane near 3.2 μm [80]. Reproduced with permission from Optical Society of America.

power of single-mode III–V diode lasers. The infrared output can be increased, however, by using optical semiconductor amplifiers to boost the output power of the single-mode diode lasers [79], or by placing the nonlinear crystal in an external buildup cavity [80] or in the laser cavity [81] of one of the pump lasers (intracavity DFG). Simon *et al.* [79] obtained as much as 50 μW of CW infrared radiation tunable near 4.3 μm by mixing a diode laser injection-seeded GaAlAs tapered traveling wave optical amplifier with a $Ti:Al_2O_3$ laser in 90° type I phase-matched $AgGaS_2$. The same authors demonstrated an external cavity DFG source [80] (Fig. 9) by mixing a resonantly enhanced compact diode-pumped 1064-nm Nd:YAG laser with 15 mW from a 795-nm single-mode GaAlAs diode laser in a 5-mm 90°-cut $AgGaS_2$ crystal. With 2 μW of CW infrared output, angle-tunable from 3.16 to 3.42 μm, the source was applied to the detection of the ν_3-asymmetric stretch motion of methane.

DFG devices have also been used for the generation of ultrashort pulses in the femtosecond (fsec) time domain to study fast reaction dynamics in areas such as optoelectronics and spectroscopy. Color center lasers and OPOs (Section 9.5) have provided fsec pulse trains up to 2.5 μm, whereas DFG allows the generation of tunable fsec pulses at even longer wavelengths. Many pump probe experiments

also require independently tunable excitation and probe pulses that are precisely synchronized on an ultrafast time scale. By difference-frequency mixing the outputs of a 100-fsec colliding pulse modelocked (CPM) dye laser/amplifier and a spectrally broad 200-fsec traveling-wave dye laser (TWDL) in two 0.3-mm $LiIO_3$ crystals, Ludwig *et al.* [82] generated two 10-nJ infrared pulses in the 2.5 to 5 μm wavelength range with pulse durations of 300 fsec ($\delta\nu \sim 250$ cm^{-1}). For fixed crystal orientations, the acceptance bandwidth of the nonlinear processes was less than the spectral bandwidth of the TWDL output, that is, only part of the TWDL output was converted to the mid-infrared. Consequently, the infrared wavelength produced in the two crystals can be tuned independently by changing the respective phase-matching angle, and the IR tuning range is determined by the spectral width of the TWDL. As an application of this source to pump probe experiments, the bleaching of the interband absorption in a PbSe direct narrow-bandgap semiconductor was observed. This technique can be easily extended to other infrared wavelengths by using different pump sources or nonlinear mixing crystals. By difference-frequency mixing the outputs of a 120-fsec Ti:Al_2O_3 laser/regenerative amplifier and a 200-fsec TWDL/amplifier in $AgGaS_2$, Hamm *et al.* [83] generated 10-nJ infrared pulses in the 4.5 to 11.5 μm region with a pulse duration of 400 fsec at a repetition rate of 1 kHz. The spectral bandwidth of the two times bandwidth-limited pulses was 60 cm^{-1}. The generated IR power was limited by strong two-photon absorption of the intense Ti:Al_2O_3 laser light in the mixing crystal.

For spectroscopy of molecular rotational transitions, hyperfine transitions, and Rydberg transitions, tunable far-infrared (FIR) radiation from the GHz microwave range up to 6 THz is required. While these frequencies cannot be reached by microwave generators, DFG by mixing a fixed-frequency CO_2 laser with a tunable infrared spin-flip Raman laser in GaAs has been used to cover this spectral range [84]. Tunable FIR radiation has also been synthesized by mixing two CO_2 lasers on a metal–insulator–metal (MIM) diode [85] either by using a fixed-frequency CO_2 laser and a tunable waveguide laser (tunable over ±120 MHz) or two fixed-frequency CO_2 lasers plus tunable microwave sidebands [86]. Due to its nonlinear current–voltage characteristic, the MIM diode generates harmonics and mixing frequencies of the incident frequencies and radiates the FIR radiation in a long wire antenna pattern. Typical FIR powers of a few tens of μW have been obtained from 200 mW of CO_2 power. Using two pressure-broadened CO_2 lasers, line-tunable over several hundred lines from 9 to 10 μm (using different CO_2 isotopomers) and a microwave generator, the entire FIR region has been covered using this DFG technique [87]. These tunable FIR sources have been used primarily for highly accurate FIR measurements of stable species to serve as frequency calibration standards [88]; to measure frequencies of transient species including molecular ions for astronomical searches [89]; and to study line broadening and lineshape parameters [90] for atmospheric spectroscopy.

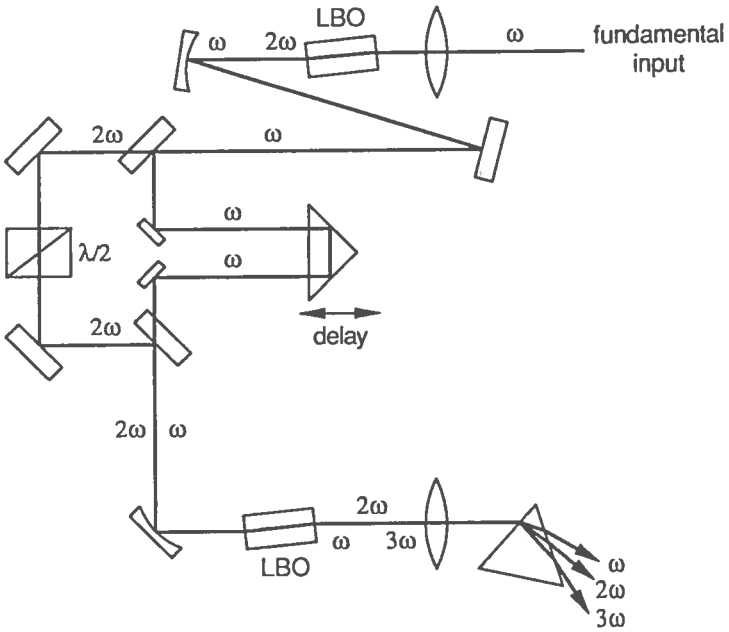

FIG. 10. THG based on two sequential second-order processes in LBO [93]. Reproduced with permission from the Optical Society of America.

9.4 Third-Harmonic Generation and Four-Wave Mixing

9.4.1 Third-Harmonic Generation as a Two-Step Process (Second-Order Parametric Interaction)

Third-harmonic generation (THG) can be performed either directly by a THG process or as a two-step process involving two sequential harmonic generation steps. In a first nonlinear crystal (doubler), a fraction of the fundamental is converted to the second harmonic. The unconverted fundamental and the second harmonic emerging from the first crystal are then coupled into the second crystal (tripler) for sum-frequency mixing. Efficient tripling requires the fundamental and the second-harmonic photons to emerge from the first crystal in a 1:1 ratio over a broad wavelength range that can be accomplished by means of an appropriate choice of polarization angle in the doubler crystal [91, 92]. In the case of short pulses, the group velocity dispersion of the fundamental and second-harmonic waves in the SFG process must be taken into account using a delay line. Figure 10 shows a typical experimental setup for THG of psec pulses [93].

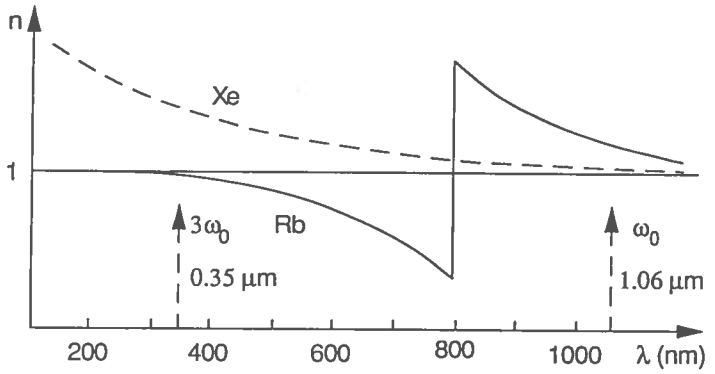

FIG. 11. Refractive indices of rubidium vapor and xenon, illustrating the THG phase-matching principle in centrosymmetric media [95]. Reproduced with permission from Springer-Verlag.

9.4.2 Four-Wave Mixing Interactions (Third-Order Parametric Processes)

Third-order parametric processes can be observed in materials with any symmetry. However, such centrosymmetric materials as gases, liquids, and some solids have been used most commonly as third-order processes and are the lowest-order nonzero nonlinearities present in these media. Generally, the lower conversion efficiencies of the higher-order processes require high pump laser intensities. As a result, third-order processes have been used primarily for generation of radiation in the extreme VUV at wavelengths too short to be reached with second-order interactions in nonlinear optical crystals.

The plane wave phase-matching condition for third-order parametric interactions is $\Delta k = 0$. The conversion efficiency is often increased by using tightly focused beams, in which case optimal performance can require either a positive or a negative value of Δk, depending on the interaction involved (focused THG requires $\Delta k < 0$) [94]. As the isotropic media used for third-order parametric processes are nonbirefringent, alternative phase-matching techniques must be used. In gases, negative dispersion occurs near allowed transitions. Therefore, phase-matching can be accomplished by using a homogeneous mixture of a rare gas and a metal vapor with different signs of dispersion (Fig. 11). Each component makes a contribution to the wave–vector mismatch in proportion to its concentration in the mixture. The appropriate phase-matching condition is met by adjusting the relative concentration of the two gases. However, in the case of THG using focused beams, only one gas with negative dispersion (e.g., Kr or Xe) is needed. The range that can be covered by THG in gas mixtures is determined by the extent of the negative dispersion region in the nonlinear materials and can be extended far into the VUV.

The conversion efficiency can be increased significantly if resonances are present between certain energy levels of the medium and the incident and generated frequencies. The effectiveness of single-photon resonances in enhancing nonlinear processes, however, is limited because of the absorption and dispersion that accompany them. Resonances in nonlinear effects can also occur when multiples of the incident frequencies match the frequency of certain types of transitions. The most commonly used resonance is a two-photon resonance involving two successive dipole transitions between levels whose spacing matches twice the value of an incident frequency. Near two-photon resonances, the nonlinear susceptibility can increase by as much as four to eight orders of magnitude, depending on the relative linewidth of the two transitions and the input radiation, resulting in a significant increase in the generated power as the input frequency is tuned through the two-photon resonance. Resonant enhanced THG has been proved very useful in allowing effective conversion of tunable radiation from dye lasers to the VUV to provide high-brightness narrow-band sources of radiation for high-resolution spectroscopy and other applications. THG from high-power pulsed lasers has been used to generate fixed-frequency and tunable radiation at various wavelengths from 3.5 μm to 57 nm.

Four-wave sum-frequency generation (SFG) and difference-frequency generation (DFG) of the form $\omega_4 = 2\omega_1 \pm \omega_3$ and $\omega_4 = \omega_1 + \omega_2 \pm \omega_3$ can also be used to produce radiation in wavelength ranges that are inaccessible by other means. These processes can be favored over possible simultaneous THG by the use of opposite circular polarization in the two pump waves, since THG with circularly polarized pump light is forbidden by symmetry. These interactions can also be used to generate tunable radiation in resonantly enhanced processes. In this case, the pump frequency at ω_1 or the sum combination $\omega_1 + \omega_2$ is adjusted to match a suitable two-photon resonance, while the remaining pump frequency at ω_3 is varied, producing tunable generated radiation.

For the DFG process phase-matching can be achieved with focused beams in media with either sign of dispersion [94]. Therefore, the usefulness of DFG is not restricted to narrow wavelength ranges above dispersive resonances, and it has been used to generate tunable radiation over broad spectral ranges in the VUV between 140 and 200 nm in rare gases Kr and Xe [96].

Four-wave DFG has also been used to generate tunable radiation in the infrared region by using pump radiation from visible and near-infrared sources. Because the gases used in these nonlinear interactions are not absorbing at FIR wavelengths, they allow more efficient generation of tunable FIR using pump sources in the visible and near-infrared region, than can be achieved in second-order nonlinear optical processes. To date, four-wave DFG has been used to produce coherent radiation at wavelengths out to 25 μm.

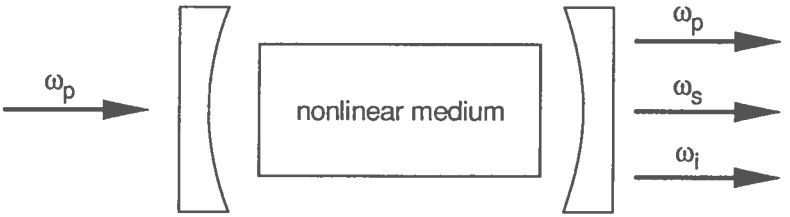

FIG. 12. Basic OPO scheme. The cavity resonates either the signal wave (singly resonant oscillator: SRO) or both signal and idler waves (doubly resonant oscillator: DRO).

9.5 Optical Parametric Amplifiers (OPAs) and Oscillators (OPOs)

9.5.1 The Optical Parametric Process

Ever since the invention of the laser, there has been a great deal of interest in the development of efficient continuously tunable coherent light sources for high-resolution spectroscopy. This field has attracted renewed interest in connection with a variety of applications in combustion diagnostics, process control, remote sensing, and environmental sensing. Picosecond and femtosecond pulses of tunable radiation are needed for time-resolved studies of chemical reactions or carrier dynamics in semiconductors. Replacement of the widely used dye and color-center lasers with more convenient sources based on Ti:sapphire and diode-pumped solid-state lasers is therefore of considerable practical utility.

OPOs [97–100] are powerful solid-state sources that provide laser radiation with potentially very large continuous-wavelength tuning ranges by parametric conversion of a fixed-frequency pump in a nonlinear optical material. Figure 12 illustrates the basic geometry of an OPO device. The nonlinear parametric interaction between the electrical field of the pump source and the nonlinear material converts pump photons at frequency ω_p in photons at frequencies ω_s (signal) and ω_i (idler) according to the conservation of energy, $\omega_p = \omega_s + \omega_i$, a process known as optical parametric amplification (OPA). For a given ω_p, there can be a continuous range of choices of ω_s and ω_i that gives rise to wavelength tunability of the parametric device. The specific pair of frequencies that will result in any given situation is determined by the conservation of momentum, or the phase-matching condition $\mathbf{k}_p = \mathbf{k}_s + \mathbf{k}_i$, with $\mathbf{k}$ the momentum vector of a wave [101]. Because the relationship between photon momentum and energy depend on the refractive index of the medium, both conditions can be simultaneously met by manipulating the refractive index of the nonlinear material, as in the case of SHG, SFG, DFG, and THG. This is usually done by using a birefringent crystalline nonlinear medium and setting the wave polarizations, crystal orientation, and temperature appropri-

ately to establish the phase-matching condition. Wavelength tuning is then achieved by changing the angle, temperature, or electric field across the crystal to modulate the effective refractive indices.

For the degenerated case in OPA ($\omega_p/2 = \omega_s = \omega_i$), the small signal gain is numerically equal to the conversion efficiency of SHG. Thus, the gain can be as high as 1% per watt of input pumping power. Although such gain is too small to be of interest for signal amplification, it can nonetheless exceed the round-trip losses in a Fabry–Perot cavity containing the gain medium, allowing coherent output to build up from a noise input. The addition of an optical cavity transforms the parametric amplifier into an optical parametric oscillator. If the optical cavity provides optical feedback for the signal wave only, it is known as a singly resonant oscillators (SRO). In this case, the threshold condition is that the parametric gain exceed twice the signal losses. For losses of 1% in the cavity, typical threshold power is on the order of 5 W. If the optical cavity provides feedback at both the signal and the idler frequencies, the device is known as a doubly resonant oscillator (DRO) and the threshold condition requires only that the gain exceed the product of signal and idler losses. The threshold power is thus lowered to tens of milliwatts at the cost of complicating the tuning behavior of the oscillator.

An OPO has several potential advantages over a laser in generating widely tunable narrow-band coherent radiation. Tuning ranges of lasers are generally limited by relatively narrow-gain bandwidths and fixed-gain centers. OPOs offer a wide wavelength operation range (0.2–18 μm) by using a solid-state nonlinear crystal as the gain medium. Since the parametric gain does not depend on any form of atomic or molecular resonances, the gain center of an OPO is tunable by changing the phase-matching, yielding a tuning range that is limited only by the dispersion and transmittance bandwidth of the nonlinear crystal. Therefore, OPOs are particularly useful when they generate radiation in spectral regions where no tunable laser sources exist (e.g., ultraviolet [102, 103], and infrared [104, 105]).

After their invention in 1965 [106, 107], early OPO development was impeded by practical difficulties related to the nonlinear optical materials, such as low optical damage thresholds and poor optical quality, as well as inadequate frequency stability of the laser pump sources. Moreover, convenient frequency control has been difficult to obtain. The sudden resurgence of interest in OPO devices is largely attributable to significant advances in the growth and fabrication of new and improved nonlinear optical materials [108]. Simultaneously, the performance of solid-state pump lasers for driving OPOs has also improved [109]. OPOs now offer the potential reliability of an all-solid-state coherent laser source. They can provide high peak power on the order of tens of MW and high average power on the order of watts with diffraction-limited beam quality. An energy conversion efficiency as high as 62% has been demonstrated [110]. The spectral bandwidth control is similar to that required for pulsed dye lasers and linewidths as small as 0.001 cm^{-1} [111] have been obtained by using etalons or injection-seeding with

TABLE II. Characterstics and Phase-Matching Ranges for OPO Materials [171]

Material	Transmission range (μm)	Phase-matching range (μm) 0.266 μm pump	0.355 μm pump	0.532 μm pump	1.064 μm pump	2.05 μm pump	Nonlinear figure of merit C^2 $(GW)^{-1}$	Optical damage threshold (GW/cm^2)
BBO	0.19–2.56	0.3–2.5	0.415–2.5	0.67–2.5	–	–	40	~1.5
LBO	0.16–2.6	0.3–2.5	0.41–2.5	0.67–2.5	–	–	5.4	~2.0
$KNbO_3$	0.35–4.2	–	–	0.61–4.2	1.43–4.2	–	44	~1.2
KTP	0.35–4.0	–	–	0.61–4.0	1.45–4.0	–	45	~1.5
$LiNbO_3$	0.35–4.3	–	–	0.61–4.3	1.42–4.3	–	15	~0.20
$AgGaS_2$	0.8–9.0	–	–	1.2–9.0	2.6–9.0	75	~0.040	
$AgGaSe_2$	1.0–15	–	–	–	2.4–15	100	~0.040	
$ZnGeP_2$	2.0–8.0	–	–	–	~2.7–8	270	~0.040	

single-mode diode lasers. They have also proven ideal for OPAs since the parametric gain is polarized, forward-directed, and bandwidth-limited, thus avoiding the superfluorescence problems associated with dye laser amplifiers.

9.5.2 OPA/OPO Materials

As increasingly sophisticated frequency-conversion applications require operation at higher efficiencies over a broader range of peak and average power and over extended spectral ranges, the demands on nonlinear materials place increasing emphasis on parameters other than birefringence and nonlinear susceptibility [112]. Notable among these are low absorption and scatter losses, high surface damage threshold, high thermal conductivity, low thermooptic coefficients, and environmental stability. Another, often crucial, issue is ease of crystal growth and processing.

Early OPOs tended to operate in the infrared wavelength region with $LiNbO_3$ as the most commonly used nonlinear optical material. During the last decade, the range of viable OPO materials has increased, as discussed in connection with SHG, SFG, and DFG. The parametric tuning range in a given crystal is determined by the pump wavelength, the transparency of the crystal, and the range over which phase-matching can be achieved. Table II summarizes the properties of nonlinear optical materials for OPAs/OPOs. These materials collectively provide good coverage of the entire wavelength region from the infrared to the UV. Most of the materials listed have a significantly higher nonlinear coefficient than $LiNbO_3$; all have equal or higher optical damage thresholds. The OPO performance can be related to the figure of merit (C^2). The single-pass optical gain G through the

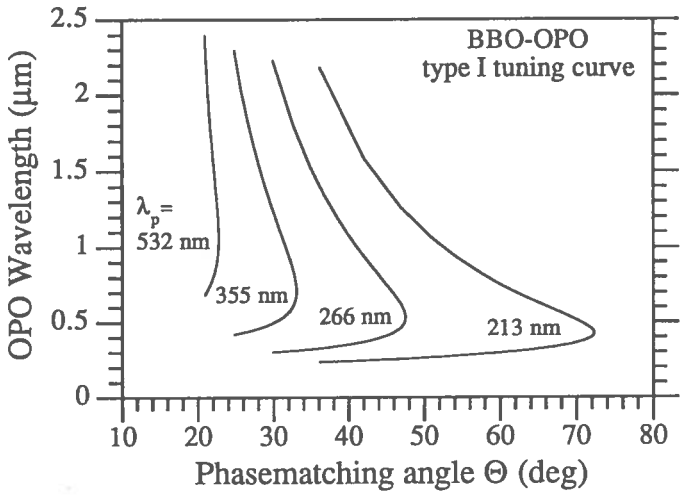

FIG. 13. Calculated wavelength tuning characteristics of a BBO OPO pumped by the second to fifth harmonic of an Nd:YAG laser. The Sellmeier equations for BBO are taken from reference [61]. Reproduced with permission from the IEEE.

crystal is given by $G = \sqrt{c^2 L^2 I_p}$, where L is the conversion length and I_p the intensity of the pump laser. As an example, Fig. 13 demonstrates the calculated wavelength tuning characteristics of a BBO OPO as a function of the phase-matching angle, pumped by the second to fifth harmonic of an Nd:YAG laser.

For the ultraviolet and visible regions, the borates BBO [102, 103, 113–119] and LBO [117–121] are the materials of choice for OPO applications. Although the smaller birefringence in LBO as compared to BBO tends to limit the phase-matching spectral range and leads to smaller tuning rates $\partial\lambda/\partial\Theta$ (requiring large-aperture crystals), it results in inherently narrower OPO linewidths and larger acceptance angles. Relatively high efficiencies can be maintained over the entire tuning range in the UV by temperature tuning the LBO OPO under noncritical phase-matching.

From the deep red to about 4.5 μm, the nonlinear crystal KTP [122–130] can be phase-matched and meets many of the key requirements for high-efficiency OPO applications, including applications in the femtosecond regime.

The large nonlinear coefficients and extended infrared transparency ranges make chalcopyrite crystals an important class for OPA/OPO work. However, the useful crystals in this family that are phase-matchable for nonlinear processes in the infrared region—$ZnGeP_2$ [131, 132], $AgGaS_2$ [133–135], and $AgGaSe_2$ [136–138]—suffer from lower optical damage intensities. However, a very attractive

feature is the possibility of tuning the entire IR range from 2.3 to 18 μm using only a single $AgGaSe_2$ crystal [136] pumped by a *Q*-switched 2.05-μm Ho:YLF laser.

With suitable nonlinear optical crystals and pump sources, virtually any wavelength ranging from the UV to the infrared can now be reached with OPOs. The technology is better developed for the near-UV to 4.5 μm range, largely due to the availability of large high-quality BBO, LBO, MgO:$LiNbO_3$, and KTP crystals. As in the case of SHG, quasi-phase-matching (Section 9.2.5) promises to impact the development of periodically poled OPOs and the use of such materials as GaAs and ZnSe [139, 140] with very high figures of merit. Simultaneously, developments in organic nonlinear materials (single-crystal and polymeric media) with outstanding promise for extremely large nonlinear susceptibilities designed with molecular-engineering techniques suggest that practical applications will grow rapidly in the future [141].

9.5.3 Pump Laser Sources

Unlike conventional lasers, OPAs/OPOs require diffraction-limited pump radiation. High peak pump powers are required for the OPO to operate well above threshold, so that parametric oscillation can build up from noise during the pump pulse. As the OPO begins to oscillate, the pump power is converted to signal and idler power, thereby depleting the pump. Thus, an ideal OPO pump laser delivers good beam quality, high peak power and pulse energy, and a high pulse repetition rate to yield high average pump power. Also, narrow bandwidth is critical for pumping narrow-band OPOs.

The primary type of pump laser for OPOs remains the lamp-pumped Nd:YAG laser (using first and higher harmonics). Most existing OPOs use Nd:YAG pump lasers operating in the *Q*-switched (nsec), modelocked (psec), or femtosecond pulse regimes [142]. Dielectric graded reflectivity nonstable optical resonators provide large-size flat-topped TEM_{00}-output beams of high quality while simultaneously providing excellent near-field beam uniformity and high spatial extraction efficiency [143].

As the peak power stability of the pump laser leads to a corresponding stability in OPO output, advances in lasers with improved spatial and temporal coherence result in more stable OPO operation. In particular, the CW single-axial mode sub-kHz-linewidth output from diode laser-pumped monolithic nonplanar Nd:YAG laser ring oscillators [144–146] has proven ideal for pumping highly stable OPOs. To produce high peak powers while maintaining good spatial and temporal coherence for pumping OPOs, the nonplanar ring resonator has been long-pulse amplified [147] or used to injection seed an 18-W CW lamp-pumped Nd:YAG oscillator [148].

Excimer lasers can also serve as pump sources for OPOs as they provide a number of ultraviolet wavelengths at relatively high overall efficiencies and high

average power levels. BBO [102, 149] and LBO [117, 150] OPOs pumped with narrow-band injection-seeded XeCl or KrF excimer lasers with narrow-linewidth and low-divergence-angle output have been demonstrated. The achievable optical-to-optical efficiencies are comparable to Nd:YAG laser-pumped OPOs for comparable pump beams. The linewidth of the output, however, is nearly an order of magnitude larger for excimer laser-pumped OPOs than for Nd:YAG laser-pumped OPOs.

A variety of other lasers—e.g., argon ion, dye, CO_2, copper vapor, color-center, He–Ne, diode, and Ti:sapphire—have achieved widespread use in research, industrial, and commercial applications. While almost all of these laser types have served as pumps for nonlinear optical devices, the Ti:sapphire lasers (particularly for generation of ultrashort pulses), diode lasers, and solid-state lasers pumped by diode lasers stand out as particularly important for contemporary developments.

9.5.4 Narrow Linewidth and Frequency Control

Many applications such as high-resolution spectroscopy, lidar, and remote-sensing require continuously tunable single-frequency light sources. In general, OPO spectral linewidths are set by the oscillator gain bandwidth (which in turn is determined by the birefringence, dispersion, and length of the crystal) and the spectral and angular spread of the pump laser beam [102, 151]. OPO linewidths are usually fairly broad, typically a few to many hundreds of wavenumbers, and often vary as a function of wavelength. Narrow-linewidth operation is achieved by providing active control for the signal and/or idler waves, either by inserting intracavity dispersive elements [152, 153] or injection seeding radiation from another narrow-band laser source [113, 154]. Type II phase-matching, known to lead to narrower linewidth than type I phase-matching [151], has also been used to generate narrow-band tunable radiational.

The use of intracavity dispersive elements in much the same way as in pulsed dye lasers led Bosenberg and Guyer [153] to a KTP OPO (Fig. 14) that produced single-longitudinal-mode single-frequency pulses ($\tau \approx 3.5$ nsec) over the range of 690 to 950 nm (signal) and 1.4 to 2.2 μn (idler) with a significantly reduced near-transform-limited bandwidth of 200 MHz. The SRO, which was pumped by the second harmonic of an injection-seeded single-mode 10-Hz Q-switched Nd:YAG laser, combined a grazing-incidence-grating resonator (Littman configuration) with an active-servo resonator-length control scheme and allowed continuous single-mode scans without mode hops of up to 100 cm^{-1}. It operated with up to 3 mJ of output, corresponding to an external photon conversion efficiency of 12%. Due to the lower efficiency of the grating at grazing incidence, the oscillator threshold was significantly higher than for an oscillator using the first-order Littrow configurational. The improvement in linewidth, however, makes the Littman design a good option for high-resolution applications.

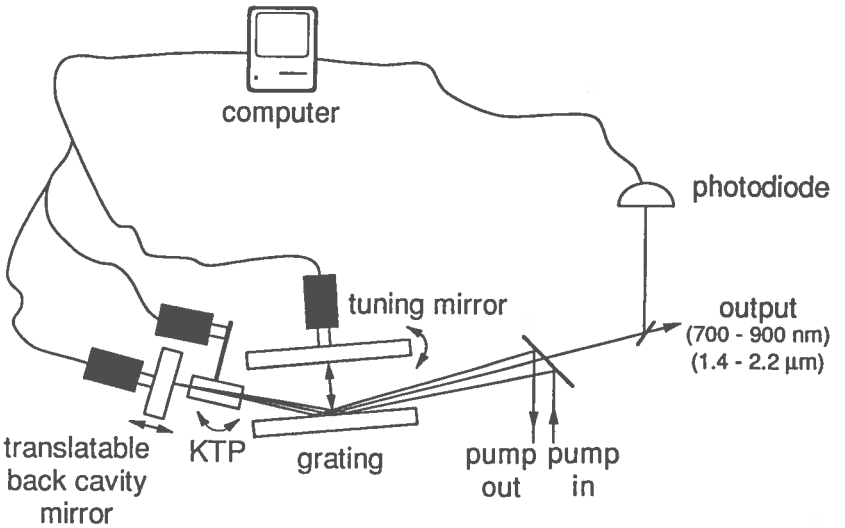

FIG. 14. OPO setup for generation of wavelength-tunable radiation with near-transform-limited bandwidth ($\Delta\nu \approx 100$ MHz) [153]. Reproduced with permission from the American Institute of Physics. A diffraction grating in Littman configuration serves as a frequency-selective element in the OPO cavity.

Haub *at el.* [154] demonstrated a BBO OPO with an effective infrared linewidth of 4 GHz and continuous tuning over ~30 cm^{-1}. The singly resonant OPO was pumped by a frequency-tripled Q-switched ($\tau = 5$ nsec) Nd:YAG laser and seeded at its visible signal wavelength with light from a tunable narrow-band (2 GHz) pulsed Rh6G dye laser. Less than 0.1 mJ dye laser energy per pulse was necessary to lock the OPO to the seed laser. For 100 mJ of 355-nm pump energy, typical pulse energies were ~20 and ~12 mJ for the idler and signal, respectively. The application of this source to rotationally resolved coherent anti-Stokes Raman spectroscopy (CARS) of N_2 in ambient air has been demonstrated [156].

Using a two-crystal walkoff compensated scheme [89], along with crystals cut for type II interaction, Bosenberg *et al.* [103] demonstrated a 355-nm pumped BBO OPO tunable from 480 to 630 nm and from 810 to 1360 nm with linewidths varying from 2 to 8 cm^{-1} over the entire tuning range without narrowing optical elements. Conversion efficiencies of 12% have been achieved with this design.

These examples show that OPOs can be efficient, broadly tunable, and narrow-band sources of coherent radiation.

9.5.5 Short-Pulse OPOs

Nanosecond pumping appears to provide the simplest method to reach the threshold of efficient parametric oscillation [102, 113, 152, 154, 157]. Nanosecond

OPOs that presently cover the wavelength region from 400 nm to 3.5 μm have been reported [158]. For example, the highly efficient nsec OPO reported by Wang *et al.* [115] was pumped by a 30-Hz *Q*-switched frequency-tripled Nd:YAG laser. The OPO used a 10-mm BBO crystal to generate continuously tunable radiation from 415 to 2400 nm. Using a double-pass pump configuration to return the undepleted portion of the pump beam back into the OPO cavity, quantum efficiencies as high as 57% and average output powers up to 507 mW at the signal wavelength 490 nm have been demonstrated from this compact continuously tunable oscillator. The exceptionally broad tuning range, ease of operation, high conversion efficiency, and potentially high output powers attainable from this OPO device make it a very practical and competitive alternative to tunable dye laser sources.

Nanosecond OPO systems have been most successful where materials with relatively high damage threshold resistance can be used [159]. For low-damage-threshold materials it is common to move to even shorter pump pulselengths. Modelocked synchronous pumping of OPOs (with the materials of choice being BBO and KTP) provides high peak power to bring the process above threshold and high average power to maximize the OPO output. For the same pump pulse energy, the peak power of the pulse can be very much higher, and thus more efficient pumping of the OPO can be achieved. Pump pulselengths are typically 5 to 100 psec, allowing peak pump powers well above the level of nsec systems without causing crystal damage. As the pulselength of a single modelocked pump pulse is too short to allow oscillation buildup, synchronous pumping of the nonlinear medium is required, for example, the total time for signal or idler waves to make a cavity round trip is equal to the modelocked pump pulse separation. When the OPO and pump laser cavities are synchronized, the circulating signal and idler pulses interact with multiple pump pulses during successive cavity round trips, allowing adequate buildup and thus high OPO efficiency. Figure 15 shows an example of a temperature-tuned LBO SRO synchronously pumped at 523 nm (Nd:YLF) [121]. The OPO was tunable from 652 to 2650 nm with four-color operation over an extensive portion of the wavelength range. An oscillation threshold of ~2.5 GW/cm^2 and an internal conversion efficiency of 20% were achieved. Guyer and Lowenthal [160] demonstrated an efficient synchronously pumped two-stage OPO driven by a modelocked and *Q*-switched Nd:YAG laser at 1.064 μm. KTP was used in the first OPO stage to degenerately down-convert the 1.064-μm pulses to 2.128 μm with ~55% conversion efficiency (signal plus idler). This first OPO stage was nearly nonresonant, with high parametric gain and ~95% output coupling, yielding extremely stable operation. Normally, a degenerate OPO has a large frequency bandwidth. However, in KTP the phase-matching must be type II, and this provides a narrow bandwidth of approximately 5 cm^{-1} at degeneracy. This fact is extremely important for driving subsequent nonlinear stages. The signal and idler 2.128-μm power was then used to drive the second

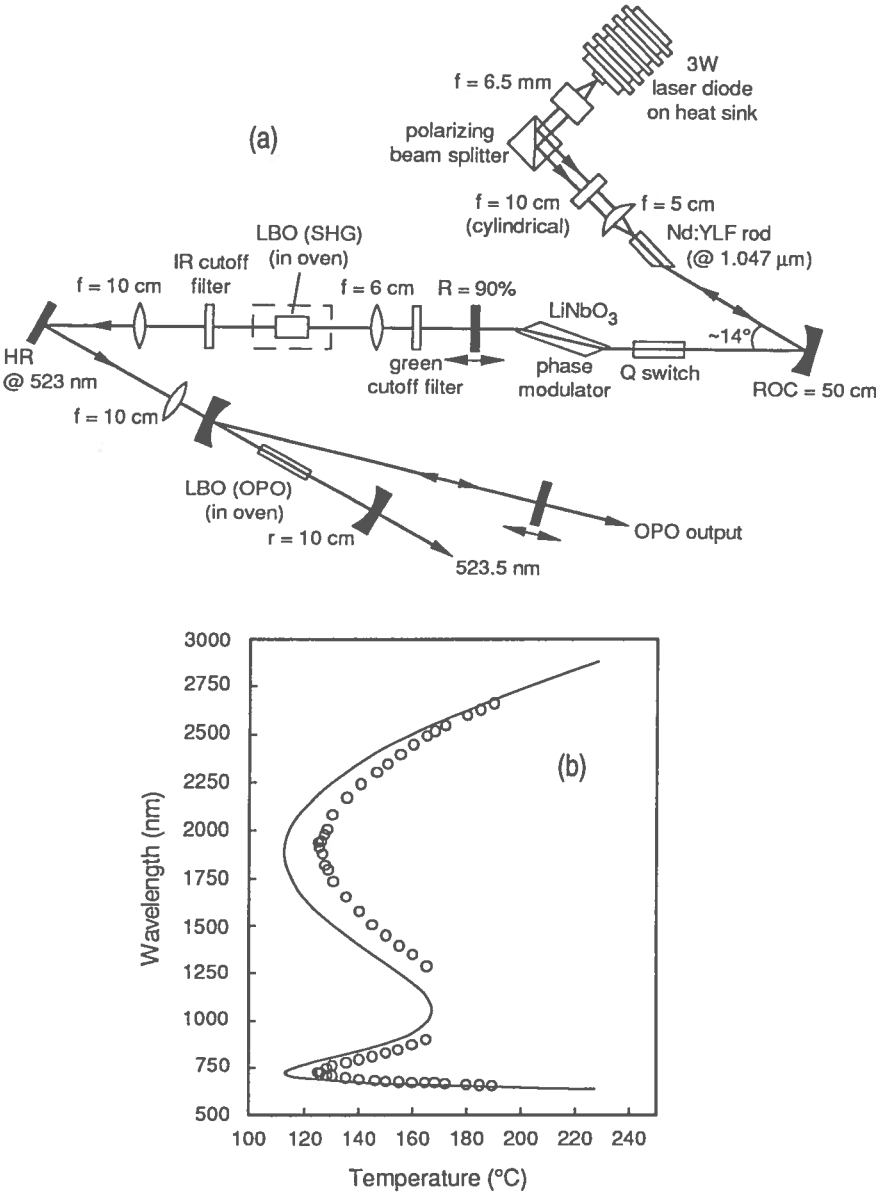

FIG. 15. (a) Setup of a synchronously pumped temperature-tuned LBO OPO [121]. Reproduced with permission from the Optical Society of America. (b) Dependence of the OPO wavelength as a function of the temperature for the LBO SRO with four-color operation over an extensive portion of the tuning range.

$AgGaSe_2$ mid-IR OPO stage. This stage achieved power conversion efficiencies of over 40% (2.128 μm converting to 3.8 and 4.8 μm) [105]. The temporal properties of a short turn-on time (2–3 nsec) and a low pulse-to-pulse temporal jitter (<500 psec) make OPOs particularly attractive devices for these multistage mixing experiments.

The synchronous pumping scheme has also been used for the generation of very short OPO output pulses required for studies of ultrafast processes in such diverse areas as physics, chemistry, electronics, and biology. Because of possible pulse broadening due to group velocity dispersion (GVD) in the nonlinear medium, the effective interaction length for femtosecond pulses is severely restricted to the order of several mm or less [161]. Thus, KTP is the prime candidate for such an application because of its relatively large effective nonlinear coefficient and small GVD. However, to reach the OPO threshold the KTP crystal must be synchronously pumped at an intracavity focus of the pump laser cavity. The intracavity fsec KTP OPO demonstrated by Edelstein *et al.* [162] provided 105-fsec short pulses at a 100-MHz repetition rate in the deep red at the mW level using a colliding-pulse modelocked (CPM) Rh6G dye laser as the pump source (τ = 170 fsec). With one set of mirrors, the OPO output was tunable from 820 to 920 nm and from 1.92 to 2.54 μm. With three additional sets of mirrors, the entire range from 700 nm to 4.5 μm can be covered. Externally pumped by a self-modelocked 125-fsec Ti:Al_2O_3 laser, a high-power high-repetition-rate fsec KTP OPO yielded an ultrashort nearly transform-limited OPO output (57 fsec) at a power level of 115 mW, tunable in the infrared region where ultrafast dye or Ti:Al_2O_3 lasers are not available [163].

9.5.6 Continuous-Wave OPOs

For many applications such as high-resolution laser spectroscopy and optical frequency division applications, a continuously tunable source with single-mode CW output and narrow linewidth is desirable. Significant progress has been made to develop OPO devices with reduced threshold energies. Two of the most commonly used low-threshold schemes that finally resulted in CW OPO operation are DROs, as well as SROs, with double-passed pump beam. CW OPOs offer the potential for widely tunable output that preserves the coherence of the pump laser source.

A DRO resonates both the signal and idler waves. As the OPO threshold is proportional to the product of the signal and idler losses, this device has a lower pump threshold than an SRO. Doubly resonant CW OPOs have been operated at high efficiency and narrow linewidth [164, 165]. However, as DROs are over-constrained by the requirements of energy conservation, phase-matching, and simultaneous cavity resonances at both signal and idler waves, perturbations on the pump frequency or OPO cavity length can cause large power fluctuations and

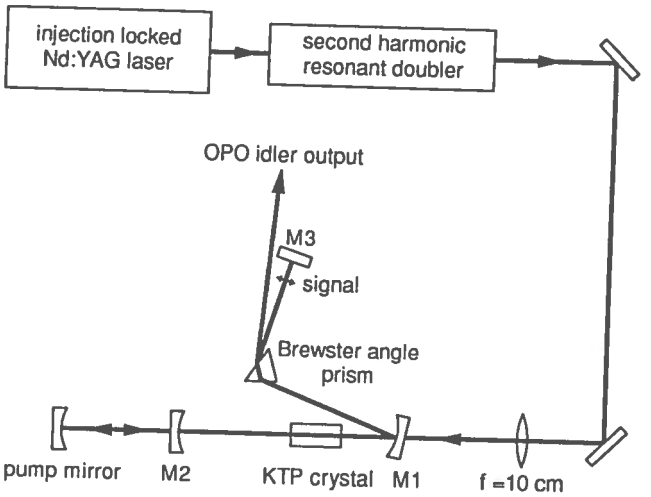

FIG. 16. Continuous-wave singly resonant KTP OPO [167]. Reproduced with permission from the Optical Society of America. Double-passing the pump wave reduces the threshold to a fourth of the calculated single-pass OPO threshold value.

mode hopping of the OPO output [166]. The monolithic ring cavity MgO:$LiNbO_3$ OPO developed by Nabors *et al.* [164] was operated near degeneracy and showed low cavity losses and good cavity length stability that are important for efficient and stable DRO operation. Pump laser stability was achieved by using the frequency-doubled output of a CW single-axial-mode diode laser-pumped monolithic Nd:YAG nonplanar ring laser. The threshold for CW OPO operation was 10 mW. With a total output power of ~8 mW, the DRO achieved 34% conversion efficiency from 532 nm pump light to signal and idler power. Wavelength tuning over 10 THz was achieved by varying the electric field applied to the nonlinear MgO:$LiNbO_3$ crystal. The OPO operated single frequency with a linewidth reproducing the 10-kHz linewidth of the pump laser source. At degeneracy, where the two output frequencies are at the subharmonic of the pump frequency, the OPO subharmonic output was found to phase lock to the pump phase to form an optical frequency divider [167]. The frequency tuning characteristics of the CW monolithic OPO have been studied theoretically in detail [142]. It appears that by tuning two variables simultaneously, such as the voltage and the pump frequency, the DRO can be continuously tuned over 10 GHz without axial mode jumps.

SROs resonate only the signal wave generated in the parametric process. Therefore, SRO designs show higher thresholds than DRO designs but result in wider and smoother OPO tuning ranges. A CW singly resonant KTP OPO (Fig. 16) demonstrated by Yang *et al.* [168] produced up to ~1 W of idler and 36 mW

of signal output with 3.2 W of pump input from a frequency-doubled injection-locked Nd:YAG laser, representing a total OPO power conversion efficiency of ~35%. By double-passing the pump through the crystal, they achieved a threshold of 1.4 W, which corresponds to a fourth of the calculated single-pass OPO threshold [169]. This device is much less susceptible to cavity-length and pump-frequency fluctuations than a doubly resonant OPO.

A CW OPO using temperature-tuned noncritically phase-matched LBO and resonating all three waves was demonstrated by Colville *et al.* [170]. As the OPO threshold pump power scales as the third power of the pump wavelength (i.e., $P_p^{th} \sim \lambda^3$), pumping the OPO in the UV at 364 nm (Ar^+ laser) resulted in a low pump power threshold of 115 mW. Wavelength tunable from 502 to 494 nm and from 1.32 to 1.38 μm, the OPO provided a maximum of 103 mW total CW OPO output (signal and idler) for 1.1 W of incident pump power, corresponding to an external conversion efficiency of ~10%.

9.6 Raman Shifters

Raman shifters are based on the stimulated Raman scattering (SRS) process [172] and provide an attractive simple and efficient means of up- and down-shifting the frequency of intense laser sources by a multiple of a Raman-active molecular transition. In this nonlinear interaction, an incident pump wave at frequency ν_p is converted to a scattered wave at a frequency $\nu_S = \nu_p - m\nu_{mol}$ (Stokes wave) or $\nu_{AS} = \nu_p + m\nu_{mol}$ (anti-Stokes wave), where m is a positive integer, and the difference in photon energy is being taken up or supplied by the nonlinear medium, which undergoes a transition with frequency ν_{mol} between two internal molecular energy states. Most commonly used forms of Raman shifters involve interactions with molecular vibrations in high-pressure gases or in liquids (ν_{mol} = 600–4155 cm^{-1}) or molecular rotations in high-pressure gases ($\nu_{mol} \approx$ 10–450 cm^{-1}) (Table III). The generated scattered wave has exponential growth, with the gain being proportional to the propagating distance and to the pump laser intensity. Phase-matching is generally not required for this stimulated processes, since the phase of the molecular excitation adjusts itself for maximum gain automatically. Figure 17 shows a typical Raman shifter setup. The output of a pulsed tunable dye laser is focused into a capillary waveguide cell (length ~50 cm) containing compressed hydrogen gas at ~40 atm [173], allowing the observation of several Stokes and anti-Stokes orders for a given incident pump wavelength. The waveguide extends the focal region, thereby increasing the gain length. Due to the large Raman shift of 4155 cm^{-1} in H_2, the use of several dyes in combination with a dye laser frequency doubler allowed the generation of various Stokes and anti-Stokes bands covering the entire wavelength range from 185 to 880 nm [174] and from 0.7 to 7 μm [175] without gaps. Mannik and Brown [173] observed an

TABLE III. Typical Raman Media

Material	$\Delta\nu$ (cm^{-1})		Gain $g \times 10^3$ (cm/MW)	
Liquids				
Benzene	992		3	
Water	3290		0.14	
N_2	2326		17	
O_2	1555		16	
Gases				
Methane	2916		0.66	(10 atm, 500 nm)
Hydrogen	4155	(vibrational)	1.5	(above 10 atm)
	450	(rotational)	0.5	(above 0.5 atm)
Deuterium	2991	(vibrational)	1.1	(above 10 atm)
N_2	2326	0.071 (10 atm, 500 nm)		
O_2	1555	0.016 (10 atm, 500 nm)		

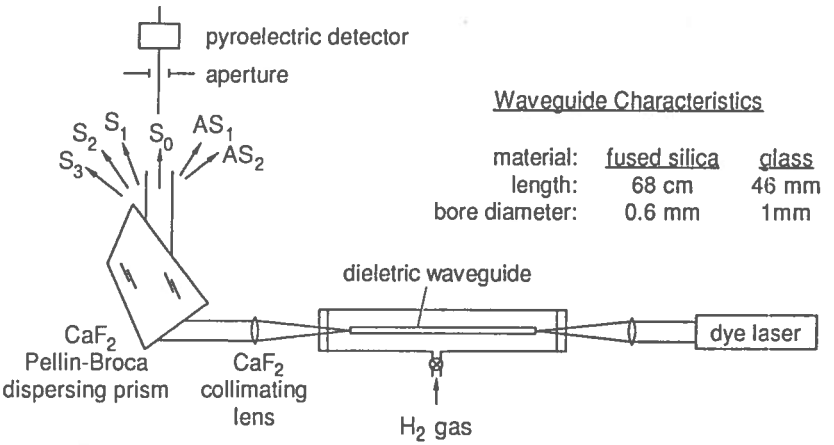

FIG. 17. Raman waveguide shifter using a high-pressure H_2 cell. The output of a frequency-doubled Nd:YAG laser pumps a dye oscillator and amplifier configuration whose output is focused into the waveguide containing 30-atm H_2 [173]. Reproduced with permission from Elsevier Science B.V.

infrared energy of 2.5 mJ generated in the third-order Stokes wave S_3 at 2 μm by guided-wave Raman shifting a 568-nm dye laser (62 mJ) with an energy conversion efficiency of ~4%. Using a Raman oscillator/waveguide-amplifier scheme to control the divergence of the Stokes beams, Hanna and Pacheco [176] demonstrated ~9% energy conversion efficiency to S_3 (1.58 μm) from 20 mJ input energy (532 nm) with H_2 as the Raman medium.

CO_2 lasers (9–11 μm), CO lasers (5 μm), or HF/DF lasers (2.5–4 μm) can also be used as intense pump sources for Raman-active media to cover large portions of the infrared wavelength region. Pumping liquid N_2 or O_2 as the Raman medium with the pressure-broadened tunable lines of HF and DF lasers allows the generation of tunable infrared coherent radiation from 5 to 10 μm for infrared spectroscopy [177, 178].

9.7 Up-Conversion Lasers

Up-conversion lasers [179] represent a class of optically pumped lasers that use nonlinear excitation processes to oscillate at frequencies higher than those used for pumping. Thus, up-conversion pumping is an alternative to using parametric nonlinear optical processes for converting infrared laser radiation to coherent output at shorter wavelengths. A number of up-conversion lasers has been demonstrated using trivalent rear-earth ions doped into crystals and glasses at sites lacking inversion symmetry as the laser medium. The interest in up-conversion lasers is motivated, to a substantial degree, by the availability of high-power red and near-infrared III–V semiconductor diode lasers that operate in spectral regions required for pumping compact solid-state up-conversion systems with wavelengths from the UV to the red for a wide range of applications.

By making use of a long-lived intermediate energy level positioned between the ground state and the upper laser level, nonlinear excitation can proceed in steps, with the intermediate state acting as a reservoir for the pump energy. In suitable laser materials, these metastable intermediate levels can be populated effectively so that they can hold as much population as, or more than, the ground state. Particularly attractive level structures for up-conversion lasing are found in Pr^{3+}, Nd^{3+}, Ho^{3+}, Er^{3+}, and Tm^{3+}. Three mechanisms can lead to efficient up-conversion excitation (Fig. 18):

a. A sequential two-step photon absorption process. In this case, up-conversion excitation is achieved with a first photon populating an intermediate metastable state and a second photon, which in the most general case would be of different energy, pumping the upper laser level via excited-state absorption [180, 181].

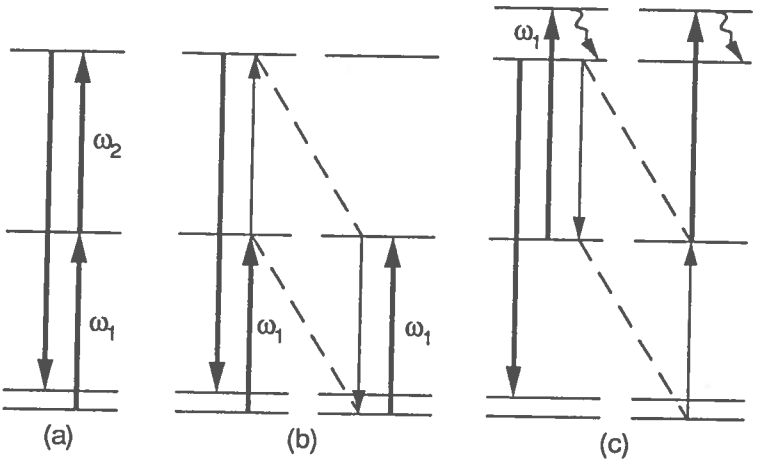

FIG. 18. Schematic of three up-conversion processes: (a) sequential two-step photon absorption, (b) the cross-relaxation process, and (c) the avalanche absorption process [179]. Reproduced with permission from the Optical Society of America.

b. A cross-relaxation process. The energy transfer between excited ions can result in efficient up-conversion when a sufficiently large number of ions has been excited to an intermediate state. Two ions in close physical proximity are coupled by a nonradiative process (electrical dipole–dipole interaction) in which one ion returns to the ground state while the other ion is promoted to the upper level. Phonons can participate in these energy transfer processes to make up for any mismatch between the energy of the donor and acceptor ions. Energy transfer processes can permit up-conversion excitation using a single pump laser that populates a long-lived intermediate state [182–184].

c. An avalanche absorption process. This process involves excited-state absorption of the pump light as well as interionic cross-relaxation and can provide efficient up-conversion pumping with a single laser. It is characteristic of this up-conversion process that the pump radiation is predominantly absorbed by excited-state absorption from an intermediate state that is populated via cross-relaxation by energy transfer [185].

The majority of the up-conversion lasers are operated at cryogenic temperatures, which is a practical disadvantage. At higher temperatures, spectral broadening leads to a reduction in the peak emission and absorption cross-sections, which in turn requires a higher inversion population to overcome laser losses and, at the same time, decreases pump absorption efficiency. The most successful approach to room-temperature up-conversion laser operation has been the use of fluoride

glass optical fibers as laser media. Fibers offer important advantages for operating CW up-conversion lasers at ambient temperature on the basis of tight optical confinement and long interaction lengths (typically on the order of 1 m) that result in high excitation density and efficient pump absorption. In addition, depletion of the population of the ground-state manifold can lead to significant reduction of self-absorption losses. The use of CW pump sources is particularly effective for populating the metastable intermediate states due to the integrating effect associated with the long lifetimes of these states. In most cases, the rear-earth ion concentration is low (several percent), and sequential two-step photon absorption rather than energy transfer processes are used for up-conversion excitation. The first CW up-conversion laser operating at room temperature was demonstrated in 1990 by Allain *et al.* [186] by pumping an Ho_3^+-doped fluorozirconate fiber with the 647-nm line of a Kr^+ laser using doubly resonant sequential two-step photon absorption. Up to 10 mW of green 550-nm output was obtained from 300 mW of red pump power. By using an intracavity prism, the green output could be tuned over ~10 nm. A Pr^{3+}-doped 1.2-m fluorozirconate fiber laser pumped by two $Ti:Al_2O_3$ lasers at 1.01 and 0.835 μm was used to demonstrate a room-temperature CW up-conversion laser operation at blue, green, orange, and red wavelengths [181]. For 1 W at 1.01 μm, the slope efficiency of generated red light (605 nm) versus pump light (835 nm) was 7%, with a maximum red power output of 30 mW.

References

1. Shen, Y. R. (1984). *The Principles of Nonlinear Optics*, Wiley, New York.
2. Zernike, F. (1975). In *Methods of Experimental Physics*, Academic Press, Boston.
3. Franken, P. A., Hill, A. E., Peters, C. W., and Weinreich, G. (1961). *Phys. Rev. Lett.* 7, 118.
4. Scifres, D. R., Burnham, R. D., and Streifer, W. (1982). *Appl. Phys. Lett.* **41**, 118.
5. Kane, T. J., and Byer, R. L. (1985). *Opt. Lett.* **10**, 65.
6. Walpole, J. N., Kintzer, E. S., Chin, S. R., Wang, C. A., and Missagia, L. J. (1992). *Appl. Phys. Lett.* **61**, 710.
7. Goldberg, L., Mehuys, D., Surette, M. R., and Hall, D. C. (1993). *IEEE J. Quantum Electronics* **Q-29**, 2028.
8. Pelouch, W. S., Powers, P. E., and Tang, C. L. (1992). *Opt. Lett.* **17**, 1070.
9. Koechner, W. (1992). *Solid-State Laser Engineering*, Springer-Verlag, Berlin.
10. Kato, K. (1986). *IEEE J. Quantum Electronics* **QE-22**, 1013. A new nonlinear material, CBO, that might be able to push the short-wavelength SHG limit to 170 nm is under investigation, as described in Wu, Y., Sasaki, T., Nakai, S., Tokotani, A., Tang, H., and Cheng, C. (1993). *Appl. Phys. Lett.* **62**, 2614.
11. Boyd, G. D., and Kleinman, D. A. (1968). *J. Appl. Phys.* **39**, 3597.

12. For short pulses, however, a large acceptance bandwidth ($\Delta\nu \approx 1/(\Delta nL)$; Δn = birefringence; L = crystal length) is required in order to sustain the short pulselength in the conversion process. In this case, the bandwidth can be increased, however, by using a dispersively compensated phase-matching scheme. See Cheville, R. A., Reiten, M. T., and Halas, N. J. (1992). *Opt. Lett.* **17**, 1343; Hofmann, Th., Mossavi, K., Tittel, F. K., and Szabo, G. (1992). *Opt. Lett.* **17**, 1691, and the references therein.
13. Yariv, A. (1990). *Quantum Electronics*, New York, Wiley.
14. Baer, T. (1986). *J. Opt. Soc. Am. B* **3**, 1175.
15. Dixon, G. J. (1989). Paper FP4 in *Dig. OSA Annual Meeting*, Washington, DC.
16. Band, Y., Ackerhalt, J. R., Chin, T., Krasinski, J. S., and Papanestor, P. (1989). In *OSA Proc. Tunable Solid-State Users*, p. 101, Optical Society of America, Washington, DC.
17. Anthony, D. W., Sipes, D. L., Pier, T. J., and Ressl, M. R. (1992). *IEEE J. Quantum Electronics* **QE-28**, 1148.
18. Nagai, H., Kume, M., Otha, I., Shimizu, H., and Kazumura, M. (1992). *IEEE J. Quantum Electronics* **QE-28**, 1164.
19. Grubb, S. G., Cannon, R. S., and Dixon, G. J. (1991). Paper CFJ6 in *Tech. Dig. CLEO '91*, Anaheim, CA, Optical Society of America, Washington, DC.
20. Hemmati, H. (1992). *IEEE J. Quantum Electronics* **QE-28**, 1169.
21. Fan, T. Y., and Byer, R. L. (1987). *IEEE J. Quantum Electronics* **QE-23**, 605.
22. Ashkin, A., Boyd, G. D., and Dziedzic, J. M. (1966). *IEEE J. Quantum Electronics* **QE-2**, 109.
23. Kozlovsky, W. J., Nabors, C. D., and Byer, R. L. (1988). *IEEE J. Quantum Electronics* **QE-24**, 913.
24. Dixon, G. J., Tanner, C. E., and Wieman, C. E. (1989). *Opt. Lett.* **14**, 731.
25. Kozlovsky, W. J., Lenth, W., Latta, E. E., Moser, A., and Bona, G. L. (1990). *Appl. Phys. Lett.* **56**, 2291.
26. Drever, R. W. P., Hall, J. L., Kowalski, F. V., Hough, J., Ford, G. M., Munley, A. J., and Ward, H. (1983). *Appl. Phys. B* **31**, 97.
27. Zimmermann, C., Hänsch, T. W., Byer, R., O'Brien, S., and Welch, D. (1992). *Appl. Phys. Lett.* **61**, 2741.
28. Yang, S. T., Pohalski, C. C., Gustafson, E. K., Byer, R. L., Feigelson, R. S., Raymakers, R. J., and Route, R. K. (1991). *Opt. Lett.* **16**, 1493.
29. In type II phase-matching in a negative (positive) birefringent crystal, two incoming waves at frequency ω, one polarized as an extraordinary ray and the other as an ordinary ray, generate a wave at frequency 2ω, polarized as an ordinary (extraordinary) ray.
30. Ou, Z. Y., Pereira, S. F., Polzik, E. S., and Kimble, H. J. (1992). *Opt. Lett.* **17**, 640.
31. Nabors, C. D., Kozolovsky, W. J., and Byer, R. L. (1988). In *Proc. SPIE*, Vol. 898, *Miniature Optics and Lasers*.
32. Schiller, S., and Byer, R. L. (1993). *J. Opt. Soc. Am. B* **10**, 1696.

33. Persaud, M. A., Tolchard, J. M., and Ferguson, A. I. (1990). *IEEE J. Quantum Electronics* **QE-26**, 1253.
34. Malcolm, G. P. A., Ebrahimzadeh, M., and Ferguson, A. I. (1992). *IEEE J. Quantum Electron* **QE-28**, 1172.
35. Armstrong, J. A., Bloembergen, N., Ducuing, J., and Pershan, P. S. (1962). *Phys. Rev.* **127**, 1918; Somekh, S., and Yariv, A. (1972). *Opt. Comm.* **6**, 301.
36. Fejer, M. M. (1992). In *Guided Wave Nonlinear Optics*, D. B. Ostrowsky and R. Reinsch (eds.), p. 133, Kluwer, Dordrecht, The Netherlands.
37. Fejer, M. M., Magel, G. A., Jundt, D. H., and Byer, R. L. (1992). *IEEE J. Quantum Electronics* **QE-28**, 2631.
38. Piltch, M. S., Cantrell, C. D., and Sze, R. C. (1976). *J. Appl. Phys.* **47**, 3514.
39. Thompson, D. E., McMullen, J. D., and Anderson, D. B. (1976). *Appl. Phys. Lett.* **29**, 113.
40. Okada, M., Takizawa, K., and Ieiri, S. (1976). *Opt. Comm.* **18**, 331.
41. Mao, H., Fu, F., Wu, B., and Chen, C. (1992). *Appl. Phys. Lett.* **61**, 1148.
42. A domain is a region of one orientation direction of the spontaneous electric polarization P_S and is linked to the sign of the nonlinear coefficient.
43. Fejer, M. M., Nightingale, J. L., Magel, G. A., and Byer, R. L. (1984). *Rev. Opt. Instrum.* **55**, 1791.
44. Xue, Y. H., Ming, N. B., Zhu, J. S., and Feng, D. (1983). *Chinese Phys.* **4**, 554; Feisst, A., and Koidl, P. (1985). *Appl. Phys. Lett.* **47**, 1125.
45. Magel, G. A., Fejer, M. M., and Byer, R. L. (1990). *Appl. Phys. Lett.* **56**, 108.
46. Jundt, D. H., Magel, G. A., Fejer, M. M., and Byer, R. L. (1991). *Appl. Phys. Lett.* **59**, 2657.
47. Khanarian, G., Norwood, R. A., Haas, D., Feuer, B., and Karim, D. (1990). *Appl. Phys. Lett.* **57**, 977.
48. Levine, B. F., Bethea, C. G., and Logan, R. A. (1975). *Appl. Phys. Lett.* **26**, 375.
49. Lim, E. J., Fejer, M. M., Byer, R. L., and Kozlovsky, W. J. (1989). *Electron. Lett.* **25**, 731.
50. Webjorn, J., Laurell, F., and Arvidsson, G. (1989). *IEEE Photon. Technol. Lett.* **1**, 316.
51. Matsumoto, S., Lim, E. J., Hertz, H. M., and Fejer, M. M. (1991). *Electron. Lett.* **27**, 2040.
52. Mizuuchi, K., and Yamamoto, K. (1992). *Appl. Phys. Lett.* **60**, 1283.
53. Makio, S., Nitanda, F., Ito, K., and Sato, M. (1992). *Appl. Phys. Lett.* **61**, 3077.
54. van der Poel, C. J., Bierlein, J. D., Brown, J. B., and Colak, S. (1990). *Appl. Phys. Lett.* **57**, 2074.
55. Mizuuchi, K., Yamamoto, K., and Taniuchi, T. (1991). *Appl. Phys. Lett.* **58**, 2732.
56. Stegeman, G. I., and Seaton, C. T. (1985). *J. Appl. Phys.* **58**, R57.
57. Yamamoto, K., Mizuuchi, K., and Taniuchi, T. (1991). *Opt. Lett.* **16**, 1156; Yamamoto, K., and Mizuuchi, K. (1992). *IEEE Photon. Technol. Lett.* **4**, 435;

Yamamoto, K., Mizuuchi, K., Kitaoka, Y., and Kato, M. (1993). *Appl. Phys. Lett.* **62**, 2599.

58. Yamada, M., Nada, N., Saitoh, M., and Watanabe, K. (1993). *Appl. Phys. Lett.* **62**, 435.
59. Lim, E. J., Hertz, H. M., Bortz, M. L., and Fejer, M. M. (1991). *Appl. Phys. Lett.* **59**, 2207.
60. Laurell, F., Brown, J. B., and Bierlein, J. D. (1992). *Appl. Phys. Lett.* **60**, 1064.
61. Kato, K. (1986). *IEEE J. Quantum Electronics* **QE-22**, 1013; Kato, K. (1986). *IEEE J. Quantum Electronics* **QE-17**, 1566.
62. Hemmati, H., Bergquist, J. C., and Itano, M. W. (1983). *Opt. Lett.* **8**, 73.
63. Watanabe, M., Hayasaka, K., Imajo, H., and Urabe, S. (1991). *Appl. Phys. Lett. B* **53**, 11; Watanabe, M., Hayasaka, K., Imajo, H., and Urabe, S. (1992). *Opt. Lett.* **17**, 46.
64. Bosenberg, W. R., Pelouch, W. S., and Tang, C. L. (1989). *Appl. Phys, Lett.* **55**, 1952.
65. Watanabe, M., Hayasaka, K., Imajo, H., and Urabe, S. (1993). *Opt. Comm.* **97**, 225.
66. Mückenheim, W., Lokai, P., Burghardt, B., and Basting, D. (1988). *Appl. Phys. B* **45**, 261.
67. Heitmann, U., Kötteritzsch, M., Heitz, S., and Hese, A. (1992). *Appl. Phys. B* **55**, 419.
68. Schomburg, H., Döbele, H. F., and Rückle, B. (1983). *Appl. Phys. B* **30**, 131.
69. Hilbig, R., and Wallenstein, R. (1982). *Appl. Opt.* **21**, 913.
70. Kean, P. N., Standley, R. W., and Dixon, G. J. (1993). *Appl. Phys. Lett.* **63**, 302.
71. Risk, W. P., and Kozlovsky, W. J. (1992). *Opt. Lett.* **17**, 707.
72. Nebel, A., and Beigang, R. (1992). *Opt. Comm.* **94**, 369.
73. Pine, A. S. (1974). *J. Opt. Soc. Am. B* **64**, 1683.
74. Bawendi, M. G., Rehfuss, B. D., and Oka, T. (1990). *J. Chem. Phys.* **93**, 6200; Xu, L. W., Gabrys, C., and Oka, T. (1990). *J. Chem. Phys.* **93**, 6210.
75. Canarelli, P., Benko, Z., Curl, R. F., and Tittel, F. K. (1992). *J. Opt. Soc. Am. B* **9**, 197; Hielscher, A. H., Miller, C. E., Bayard, D. C., Simon, U., Smolka, K. P., Curl, R. F., and Tittel, F. K. (1992). *J. Opt. Soc. Am. B* **9**, 1962.
76. Miller, C. E., Simon, U., Eckhoff, W. C., Tittel, F. K., and Curl, R. F. (1993). *AIP Conf. Proc., ELICOLS '93*, Hot Springs, VA.
77. Wieman, C. E., and Hollberg, L. (1991). *Rev. Sci. Instrum.* **62**, 1.
78. Simon, U., Miller, C. E., Bradley, C. C., Hulet, R. G., Curl, R. F., and Tittel, F. K. (1993). *Opt. Lett.* **18**, 1062.
79. Simon, U., Tittel, F. K., and Goldberg, L. (1993). *Opt. Lett.* **18**, 1931.
80. Simon, U., Waltman, S., Loa, I., Tittel, F. K., and Hollberg, L. (1995). *J. Opt. Soc. Am. B* **12**, 323.
81. Effenberger, F. J., and Dixon, G. J. (1992). *Advanced Solid-State Lasers*, Topical Meeting, New Orleans, LA.
82. Ludwig, C., Frey, W., Woerner, M., and Elsaesser, T. (1993). *Opt. Comm.* **102**, 447.
83. Hamm, P., Lauterwasser, C., and Zinth, W. (1993). *Opt. Lett.* **18**, 1943.

84. Shen, Y. R., ed. (1977). *Nonlinear Infrared Generation*, Topics in Applied Physics, Volume 16, Springer, Heidelberg.

85. Evenson, K. M., Inguscio, M., and Jennings, D. A. (1985). *J. Appl. Phys.* **57**, 956.

86. Evenson, K. M., Jennings, D. A., Leopold, K. R., and Zink, L. R. (1985). *Laser Spectroscopy*, Vol. VII, T. W. Hänsch and Y. R. Shen (eds.), Springer Series on Optical Science, Volume 49, p. 366, Springer-Verlag, Heidelberg; Evenson, K. M., Jennings, D. A., and Vanek, M. D. (1988). In *Frontiers of Laser Spectroscopy of Gases*, A. C. P. Alves (eds.), p. 43, Kluwer, Dordrecht, The Netherlands.

87. Inguscio, M. (1988). *Phys. Scripta* **37**, 699; Inguscio, M., Zink, P. R., Evenson, K. M., and Jennings, D. A. (1987). *Opt. Lett.* **12**, 867.

88. Nolt, I. G., DiLonardo, G., Evenson, K. M., Hinz, A., Jennings, D. A., Leopold, K. R., Vanek, M. D., Radistitz, J. V., and Zink, L. R. (1987). *J. Mol. Spectrosc.* **125**.

89. Brown, J. M., Zink, L. R., Jennings, D. A., Evenson, K. M., Hinz, A., and Nolt, I. G. (1986). *Appl. Phys.* **307**, 210; Leopold, K. R., Zink, L. R., Evenson, K. M., and Jennings, D. A. (1986). *J. Chem. Phys.* **84**, 1935; Jennings, D. A., Evenson, K. M., Zink, L. R., Demuynck, C., Destombes, J. L., Lemoine, B., and Johns, J. W. (1986). *J. Mol. Spectrosc.* **122**, 477.

90. Jennings, D. A., Evenson, K. M., Vanek, M. D., Nolt, I. G., Radistitz. J. V., and Chance, K. V. C. (1987). *Geophys. Res. Lett.* **14**, 722.

91. Craxton, R. S. (1980). *Opt. Comm.* **34**, 474.

92. Craxton, R. S. (1981). *IEEE J. Quantum Electronics* **QE-17**, 1771.

93. Nebel, A., and Beigang, R. (1991). *Opt. Lett.* **16**, 1729.

94. Reintjes, J. F. (1990). "Nonlinear Optical Processes," in *Encyclopedia of Modern Physics*, R. A. Meyers (ed.), Academic Press, New York.

95. Demtröder, W. (1991). *Laserspektroskopie*, Springer-Verlag, Berlin.

96. Hilbig, R., and Wallenstein, R. (1982). *Appl. Opt.* **21**, 913; Hilbig, R., and Wallenstein, R. (1982). *Appl. Opt. B* **28**, 202.

97. Harris, S. E. (1969). *Proc. IEEE* **57**, 2096.

98. Byer, R. L. (1975). "Optical Parametric Oscillators," in *Treatise on Quantum Electronics*, Vol. 1: *Nonlinear Optics*, Parts A and B, H. Rabin and C. L. Tang (eds.), Academic Press, New York.

99. Tang, C. L. (1975). "Spontaneous and Stimulated Parametric Processes," *Treatise on Quantum Electronics*, Vol. 1: *Nonlinear Optics*, Parts A and B, H. Rabin and C. L. Tang (eds.), Academic Press, New York.

100. Cheng, L. K., Rosker, M. J., and Tang, C. L. (1987). In *Tunable Lasers*, L. F. Mollennauer and J. C. White (eds.), Springer-Verlag, Berlin.

101. Yariv, A. (1990). Quantum Electronics, 3rd edition, Wiley, New York.

102. Ebrahimzadeh, M. E., Henderson, A. J., and Dunn, M. H. (1990). *IEEE J. Quantum Electronics* **QE-26**, 1241.

103. Bosenberg, W. R., Cheng, L. K., and Tang, C. L. (1989). *Appl. Phys. Lett.* **54**, 13.

104. Barnes, N., and Murray, K. (1990). Unpublished lecture.

105. Guyer, D. R., Hamilton, C., Braun, F., Lowenthal, D., and Ewing, J. (1991). In *Proceedings of the Conference on Lasers and Electro-Optics*, Baltimore, MD, Technical Digest Series, Optical Society of America, Washington, DC.

106. Wang, C. C., and Racette, G. W. (1965). *Appl. Phys. Lett.* **6**, 169.

107. Giordamaine, J. A., and Miller, R. C. (1965). *Phys. Rev. Lett* **14**, 973.

108. For a list of references, see Dmitriev, V. G., Gurzadyan, G. G., and Nikogosyan, D. N. (1911). In *Handbook of Nonlinear Optical Crystals*, Vol. 64, pp. 181–191, Springer, New York.

109. Byer, R. L. (1988). *Science* **239**, 742.

110. Miyabke, C. I., Braun, F., and Guyer, D. R. (1992). In *Proc. Advanced Solid-State Laser Conference*, Optical Society of America, Washington, DC.

111. Pinard, J., and Young, J. F. (1972). *Opt. Comm.* **4**, 425.

112. Bordui, P. F., and Fejer, M. M. (1993). *Annu. Rev. Mater. Sci.* **23**, 321.

113. Fan, Y. X., Eckardt, R. C., Byer, R. L., Nolting, J., and Wallenstein, R. (1988). *Appl. Phys. Lett.* **53**, 2014; Fan, Y. X., Eckardt, R. C., Byer, R. L., Chen, C., and Jiang, A. D. (1989). *IEEE J. Quantum Electronics* **QE-25**, 1196.

114. Cheng, L. K., Bosenberg, W. R., and Tang, C. L. (1989). *Appl. Phys. Lett.* **54**, 13.

115. Wang, Y., Xu, Z., Deng, D., Zheng, W., Liu, X., Wu, B., and Chen, C. (1991). *Appl. Phys. Lett.* **58**, 1461.

116. Fix, A., Schröder, T., Wallenstein, R., Haub, J. G., Johnson, M. J., and Orr, B. J. (1993). *J. Opt. Soc. Am. B* **10**, 1744.

117. Withers, D. E., Robertson, G., Henderson, A. J., Tang, Y., Cui, Y., Sibett, W., Sinclair, B. D., and Dunn, M. H. (1993). *J. Opt. Soc. Am. B* **10**, 1737.

118. Komine, H. (1993). *J. Opt. Soc. Am. B* **10**, 1751.

119. Zhang, J. Y., Huang, J. Y., Shen, Y. R., and Chen, C. (1993). *J. Opt. Soc. Am. B* **10**, 1758.

120. Robertson, G., Henderson, A., and Dunn, M. H. (1992). *Appl. Phys. Lett.* **60**, 271.

121. Ebrahimzadeh, M. E., Hall, G. J., and Ferguson, A. I. (1992). *Opt. Lett.* **17**, 652; Ebrahimzadeh, M. E., Hall, G. J., and Ferguson, A. I. (1992). *Appl. Phys. Lett.* **60**, 1421.

122. Vanherzeele, H. (1990). *Appl. Opt.* **29**, 2246.

123. Powers, P. E., Ellington, R. J., Pelouch, W. S., and Tang, C. L. (1993). *J. Opt. Soc. Am. B* **10**, 2162.

124. Hall, G. J., Ebrahimzadeh, M., Robertson, A., Malcolm, G. P. A., and Ferguson, A. I. (1993). *J. Opt. Soc. Am. B* **10**, 2168.

125. McCarthy, M. J., and Hanna, D. C. (1993). *J. Opt. Soc. Am. B* **10**, 2180.

126. Lotshaw, W. T., Unternahrer, J. R., Kukla, M. J., Miyake, C. I., and Brown, F. D. (1993). *J. Opt. Soc. Am. B* **10**, 2191.

127. Nebel, A., Fallnich, C., Beigang, R., and Wallenstein, R. (1993). *J. Opt. Soc. Am. B* **10**, 2195.

128. Chung, J., and Siegman, A. E. (1993). *J. Opt. Soc. Am. B* **10**, 2201.

129. Apesi, A., Reali, R. C., Kubecek, V., Kumazaki, S., Takagi, Y., and Yoshihara, K. (1993). *J. Opt. Soc. Am. B* **10**, 2211.

130. Gräser, Ch., Wang, D., Beigang, R., and Wallenstein, R. (1993). *J. Opt. Soc. Am. B* **10**, 2218.

131. Vodopyanov, K. L. (1993). *J. Opt. Soc. Am. B* **10**, 1723.

132. Budni, P. A., Schunemann, P. G., Knights, M. G., Pollak, T. M., and Chicklis, E. P. (1992). In *Digest of Advanced Solid-State Lasers*, Optical Society of America, Washington, DC.

133. Fan, Y. X., Eckardt, R. C., Byer, R. L., Route, R. K., and Feigelson, R. S. (1984). *Appl. Phys. Lett.* **45**, 313.

134. Bakker, H. J., Kennis, J. T. M., Kop, H. J., and Lagendijk, A. (1991). *Opt. Comm.* **86**, 58.

135. Krause, H.-J., and Daum, W. (1993). *Appl. Phys. B* **56**, 8.

136. Eckardt, R. C., Fan, Y. X., Byer, R. L., Marquardt, C. L., Storm, M. E., and Esterowitz, L. (1986). *Appl. Phys. Lett.* **49**, 608.

137. Catella, G. C., Shiozawa, L. R., Hietanen, J. R., Eckardt, R. C., Route, R. K., Feigelson, R. S., Cooper, D. G., and Marquardt, C. L. (1993). *Appl. Opt.* **32**, 3948.

138. Budni, P. A., Knights, M. G., Chicklis, E. P., and Schepler, K. L. (1993). *Opt. Lett.* **18**, 1068.

139. Gordon, L. A., Woods, G. L., Eckardt, R. C., Route, R. K., Feigelson, R. S., Fejer, M. M., and Byer, R. L. (1993). *Electron. Lett.* **29**, 1942.

140. Gordon, L. A., Eckardt, R. C., and Byer, R. L. (1994). In *Proc. OE/LASE'94*, SPIE, Los Angeles.

141. Zyss, J. (1994). *Molecular Nonlinear Optics: Materials, Devices, and Physics*, Academic Press, Boston.

142. Eckardt, R. C., Nabors, C. D., Kozlovsky, W. J., and Byer, R. L. (1991). *J. Opt. Soc. Am. B* **8**, 646.

143. Parent, A., and Lavigne, P. (1989). *Opt. Lett.* **14**, 399.

144. Kane, T. J., and Byer, R. L. (1985). *Opt. Lett.* **10**, 65.

145. Kane, T. J., Nilsson, A. C., and Byer, R. L. (1987). *Opt. Lett.* **12**, 175.

146. Day, T., Gustafson, E. K., and Byer, R. L. (1991). *Opt. Lett.* **15**, 221.

147. Kane, T. J., Kozlovsky, W. J., and Byer, R. L. (1986). *Opt. Lett.* **11**, 216.

148. Nabors, C. D., Farinas, A. D., Day, T., Yang, S. T., Gustafson, E. K., and Byer, R. L. (1989). *Opt. Lett.* **14**, 1189.

149. Komine, H. (1988). *Opt. Lett.* **13**, 643.

150. Ebrahimzadeh, M. E., Robertson, G., and Dunn, M. H. (1991). *Opt. Lett.* **16**, 767.

151. Brosnan, S. J., and Byer, R. L. (1979). *IEEE J. Quantum Electronics* **QE-15**, 415.

152. Bosenberg, W. R., Pelouch, W. S., and Tang, C. L. (1989). *Appl. Phys. Lett.* **55**, 1952.

153. Bosenberg, W. R., and Guyer, D. R. (1992). *Appl. Phys. Lett.* **61**, 387.

154. Haub, J. G., Johnson, M. J., Orr, B. J., and Wallenstein, R. (1991). *Appl. Phys. Lett.* **58**, 1718.

155. Bosenberg, W. R., and Tang, C. L. (1990). *Appl. Phys. Lett.* **56**, 1819.

156. Johnson, M. J., Haub, J. G., Barth, H.-D., and Orr, B. J. (1993). *Opt. Lett.* **18**, 441.

157. Marshall, L. R., Kansinski, J., Hays, A. D., and Burnham, R. (1991). *Opt. Lett.* **16**, 681.

158. Tang, C. L., Bosenberg, W. R., Ukachi, T., Lane, R. J., and Cheng, L. K. (1992). *Proc. IEEE* **80**, 365.

159. Thresholds for nanosecond OPOs are higher than for CW OPO operation, which can result in crystal surface damage before the threshold intensity is reached (Section 9.5.6).

160. Guyer, D. R., and Lowenthal, D. D. (1990). *Proc. SPIE 1220, Nonlinear Optics* **41**.

161. Simultaneously, for short pulses a large acceptance bandwidth ($\Delta\nu \approx 1/(\Delta nL)$; Δn = birefringence; L = crystal length) is required in order to sustain the short pulselength in the conversion process.

162. Edelstein, D. C., Wachman, E. S., and Tang, C. L. (1989). *Appl. Phys. Lett.* **54**, 1728; Wachman, E. S., Edelstein, D. C., and Tang, C. L. (1990). *Opt. Lett.* **15**, 136.

163. Pelouch, W. S., Powers, P. E., and Tang, C. L. (1992). *Opt. Lett.* **17**, 1070.

164. Nabors, C. D., Eckardt, R. C., Kozlovsky, W. J., and Byer, R. L. (1989). *Opt. Lett.* **14**, 1134.

165. Lee, D., and Wong, N. C. (1992). *Opt. Lett.* **17**, 13.

166. Smith, R. G. (1973). *IEEE J. Quantum Electronics* **QE-9**, 530.

167. Nabors, C. D., Yang, S. T., Day, T., and Byer, R. L. (1990). *J. Opt. Soc. Am. B* **7**, 815.

168. Yang, S. T., Eckardt, R. C., and Byer, R. L. (1993). *Opt. Lett.* **18**, 971.

169. Guha, S., Wu, F. J., and Falk, J. (1982). *IEEE J. Quantum Electronics* **QE-18**, 907.

170. Colville, F. G., Henderson, A. J., Padgett, M. G., Zhang, J., and Dunn, M. H. (1993). *Opt. Lett.* **18**, 205; Colville, F. G., Padgett, M. G., Henderson, A. J., Zhang, J., and Dunn, M. H. (1993). *Opt. Lett.* **18**, 1065.

171. Bosenberg, W. R., Guyer, D. R., Lowenthal, D. D., and Moody, S. E. (1992). *Laser Focus World*, **165**, May.

172. White, J. C. (1987). In *Tunable Lasers*, L. F. Mollennauer and J. C. White (eds.), Topics in Applied Physics, Springer-Verlag, Berlin.

173. Mannik, L., and Brown, S. K. (1986). *Opt. Comm.* **57**, 360.

174. Wilke, V., and Schmidt, W. (1979). *Appl. Phys.* **18**, 177.

175. Hartig, W., and Schmidt, W. (1979). *Appl. Phys.* **18**, 235.

176. Hanna, D. C., and Pacheco, M. T. T. (1986). *Opt. Comm.* **60**, 107.

177. Grasiuk, A. Z., and Zuharev, I. G. (1978). *Appl. Phys.* **17**, 211.

178. Wellegehausen, B., Ludewigt, K., and Welling, H. (1985). *Proc. SPIE* **492**, 10.

179. Lenth, W., and Macfarlane, R. M. (1992). *Optics and Photonics News*, **8**.

180. Macfarlane, R. M., Tong, F., Silversmith, A. J., and Lenth, W. (1988). *Appl. Phys. Lett.* **52**, 1300.

181. Smart, R. G., Hanna, D. C., Tropper, A. C., Davey, S. T., Carter, S. F., and Szebesta, D. (1991). *Electron. Lett.* **27**, 1307.

182. Lenth, W., Silversmith, A. J., and Macfarlane, R. M. (1988). In *Advances in Laser Science*, Vol. 3, A. C. Tarn, J. L. Gole, and W. C. Stwalley (eds.), *AIP Confer. Proc.* **172**, 8.

183. Hebert, T., Risk, W. P., Macfarlane, R. M., and Lenth, W. (1990). In *Proc. Adv. Solid State Lasers*, Vol. 6, p. 379, H. J. Jenssen and G. Dube (eds.), Optical Society of America, Washington, DC; Hebert, T., Wannemacher, R., Lenth, W., and Macfarlane, R. M. (1990). *Appl. Phys. Lett.* **57**, 1727.

184. Macfarlane, R. M., Robinson, M., and Pollack, S. A. (1990). *Proc. SPIE* **1223**, 294.

185. Macfarlane, R. M., Wannemacher, R., Hebert, T., and Lenth, W. (1990). Paper CWF-1 in *Tech. Dig. CLEO '91*, Anaheim, CA, Optical Society of America, Washington, DC.

186. Allain, J. Y., Monerie, M., and Poignant, H. (1990). *Electron. Lett.* **26**, 166; Allain, J. Y., Monerie, M., and Poignant, H. (1990). *Electron. Lett.* **26**, 261; Allain, J. Y., Monerie, M., and Poignant, H. (1991). *Electron. Lett.* **27**, 189.